CONTRIBUTIONS OF ANGIOMOTIN-LIKE-1 ON ASTROCYTIC MORPHOLOGY: POTENTIAL ROLES IN REGULATING CONNEXIN-43-BASED ASTROCYTIC GAP JUNCTIONS, REMODELING THE ACTIN CYTOSKELETON AND INFLUENCING CELLULAR POLARITY

Nicholas Frederick Downing

Submitted to the faculty of the University Graduate School
in partial fulfillment of the requirements
for the degree
Master of Science
in the Department of Biochemistry and Molecular Biology,
Indiana University

October 2019

Accepted by the Graduate Faculty of Indiana University, in partial fulfillment of the requirements for the degree of Master of Science.

Master's Thesis Committee

Clark D. Wells, PhD, Chair

Mark G. Goebl, PhD

Lawrence A. Quilliam, PhD

ACKNOWLEDGEMENT

First and foremost, I would like to express my gratitude to Dr. Clark Wells. He has been an outstanding mentor throughout this year and has provided me with the guidance, insight and support in completing this research. His stories of graduate school, daily advice, and, of course, his genuine commitment to my professional success has had an absolutely positive impact on me and I am beyond excited to see where my future at Indiana University Bloomington takes me. In addition to my advisor, I want to thank Drs. Mark Goebl and Lawrence Quilliam for their presence on my thesis committee. They have been some of the most encouraging faculty that I have ever had the pleasure of meeting and I am forever grateful for their help in achieving my academic goals. I feel it is essential that I thank Kevin Lange for all of his assistance, technical instruction and *constructive* criticism that he has given me over the past year. Without him, much of this work would have been difficult to complete in such a brief amount of time. I wish him the best of luck in both his defense and future beyond IUSM. Lastly, I would like to thank my family for their constant support, enthusiasm and encouragement in my pursuit of a graduate education. They bring out the best in me and I don't know where I would be without them.

Nicholas Frederick Downing

CONTRIBUTIONS OF ANGIOMOTIN-LIKE-1 ON ASTROCYTIC MORPHOLOGY: POTENTIAL ROLES IN REGULATING CONNEXIN-43-BASED ASTROCYTIC GAP JUNCTIONS, REMODELING THE ACTIN CYTOSKELETON AND INFLUENCING CELLULAR POLARITY

Glioblastoma is a lethal cancer that arises from support cells in the nervous system and kills around 20,000 people in the United States each year. While much is known about the highly malignant primary glioblastoma, the natural history of lower grade glioma (LGG) is less understood. While the majority of LGGs are initiated by a mutation in isocitrate dehydrogenase, the events leading to their malignant progression into a grade IV tumor are not known. Analysis of primary tumor sample data has revealed that low transcript levels of Angiomotin-like-1 (AmotL1) strongly associate with poor outcomes of patients with these cancers. Follow-up RNA-sequencing of human embryonic astrocytes with AmotL1 silencing revealed the downregulation of many transcripts that encode proteins mediating gap junctions (GJ) between astrocytes, especially connexin-43 (Cx43). Cx43 protein oligomerizes to form functional channels comprising the astrocytic GJ. AmotL1 knockdown through RNA interference decreases Cx43 transcript and protein levels while increasing its distribution to GJs. This suggests increased GJ formation and intercellular communication, as similar localization patterns are observed in differentiated astrocytes. Astrocytes with AmotL1 knockdown also display a pronounced pancake-like morphology, suggesting that the actin cytoskeleton is affected. Imaging reveals that cells with reduced AmotL1 have characteristic losses in both stress fibers and focal actin under the cell body but notable increases in cortical F-actin. Consistent with previous studies,

AmotL1 may promote increases in the number and thickness of F-actin fibers. Because actin binding to related angiomotins is inhibited by phosphorylation from the LATs kinases, I define the effects of expressing wildtype AmotL1 versus mutants that mimic or prevent phosphorylation by LATs1/2. Interestingly, expression of AmotL1 S262D in combination with NEDD4-1, a ubiquitin ligase, results in a profound loss of actin stress fibers. Dependence on NEDD4-1 suggests that this phenotype is due to the induced degradation of proteins that promote F-actin, e.g. RhoA. These results directly support a model in which phosphorylated AmotL1 specifically inhibits F-actin formation as opposed to unphosphorylated AmotL1 which is known to promote stress fiber formation. Thus, in addition to regulating polarity and YAP/TAZ transcriptional co-activators, AmotL1 plays major functions in dictating cellular F-actin dynamics.

Clark D. Wells, PhD, Chair

TABLE OF CONTENTS

LIST OF TABLES

LIST OF FIGURES

LIST OF ABBREVIATIONS

AANS:	American Association of Neurological Surgeons
ABTA:	American Brain Tumor Association
AIP4:	Atrophin-1 interacting protein 4; an E3 ubiquitin ligase
Amot:	Angiomotin protein
AmotL1:	Angiomotin-like protein 1
Arp2/3:	actin-related protein 2/3 complex
B-TrCP:	Beta-transducin repeat containing E3 ubiquitin protein ligase
Cdc43:	Cell division control protein 42 homolog
Cx43:	Connexin-43
ECM:	Extracellular matrix
EtBr:	Ethidium bromide dye
GBM:	Glioblastoma
GJIC:	Gap junction intercellular communication
GUK:	Guanylate kinase homology domain
HBEGF:	Heparin binding epithelial EGF-like growth factor
HECT:	Homologous to the E6-AP Carboxyl Terminus; protein domain
IDH:	Isocitrate dehydrogenase
LATS1/2:	Large tumor suppressor protein 1/2
LKB1:	Liver kinase B1, also known as serine/threonine kinase 11; a tumor suppressor
LRP:	Lipoprotein receptor-related protein
NCI:	National Cancer Institute

Nedd4-1:	Neural precursor cell expressed developmentally down-regulated protein 4; a member of the AIP4 E3 ubiquitin ligase family
RNAi:	RNA interference
RNA-seq:	RNA-sequencing analysis (high throughput)
ROCK1:	Rho-associated, coiled-coil-containing kinase
SH3:	Src-homology 3 domain
siRNA:	Small-interfering RNA
shRNA:	Short-hairpin RNA
STRAD:	STE20-related kinase adaptor, LKB1-interacting protein
TCF:	T-cell factor, group of transcription factors
TGFβ:	Tumor growth factor beta
TCGA:	The Cancer Genome Atlas
WASP:	Wiskott-Aldrich syndrome protein
ZO-1:	Zona (Zonula) occludens-1, tight junction protein-1

Introduction

According to the National Cancer Institute (NCI), an estimated 23,000 Americans are diagnosed with cancer of the central nervous system each year. Of these, at least 11,500 are glioblastoma multiforme (GBM), gliomas that arise from abnormal changes in healthy glial cells (AANS, ABTA). For adults diagnosed with primary GBM, the estimated median survival is between one and three years depending on the genetic makeup of the tumor. This is because GBM initially presents as aggressive grade IV tumors (Davis 2016, Llaguno et al. 2016, ABTA). Although GBM can occur in individuals of all ages, the median age of onset is 67 years. A second type of glioma presents as a lower grade glioma (LGG). Unfortunately, many of these tumors go undiagnosed in patients until there is a manifestation of physical symptoms, such as intense headaches, nausea, blurred vision, changes in memory, sensation, balance and motor skills. These symptoms arise from brain swelling, due either to edema or from the pressure of the expanding tumor within the skull (Faivre et al. 2015). While these tumors initially present as grade II or grade III, after prolonged development, they progress into secondary grade IV tumors with a very poor patient prognosis. Grade II tumors are slow-growing and do not warrant immediate fear; with consistent monitoring and treatment, patients can be expected to have several years of high-quality life. Upon reaching grades III and IV, tumor cells de-differentiate, divide rapidly and become metastatic, invading other healthy tissues throughout the central nervous system (NCI).

The majority of lower grade gliomas contain a mutation in the isocitrate dehydrogenase 1 (*IDH1*) gene. Tumors with mutant *IDH1* have an attenuated immune response and reduced tumor aggressiveness relative to tumors with wildtype (WT) *IDH1*

(Amankuloar et al. 2017). The *IDH1* mutation which is detectable after surgical biopsy, has become a significant molecular marker in determining patient prognosis as individuals with mutant *IDH1*-positive tumors have a median survival of 29 months compared to those with WT *IDH1*, whose median survival is 13 months (ABTA). Additional work has revealed that mutant IDH1 has a neomorphic enzymatic activity that converts alpha-ketoglutarate to the oncometabolite: 2-hydroxyglutarate (2-HG) (Molenaar et al. 2018, Sulkowski et al. 2017). Accumulation of 2-HG results in the inhibition of about 70 intracellular dioxygenases that include TET DNA demethylases, Jumanji histone demethylases and EGLN prolyl hydroxylases resulting in negative consequences (Figueroa et al. 2010, Kickingereder et al. 2015). Excessive DNA methylation and HIF activation by an absence of prolyl hydroxylation are linked to secondary glioblastomas and to the progression of many tumor types, respectively (Kaur et al. 2005).

In recent years, the Wells laboratory has studied the role of a loss of angiomotin-like 1 (AmotL1) in the progression of lower grade gliomas into secondary glioblastomas. Analysis of publicly-available tumor datasets (TCGA and Rembrandt) reveals that this loss of AmotL1 may be a significant factor in promoting malignant progression. AmotL1 is a scaffolding protein that binds apical polarity proteins through its C-terminus and the YAP/TAZ transcriptional co-activators at its N-terminus (Chan et al. 2011). This allows AmotL1 to control polarity and HIPPO signaling in a zero-sum manner to promote polarity and prevent cellular growth (Wang et al. 2010). The inhibition of YAP1 occurs through both sequestration in the cytosol and induced degradation. This inhibition prevents YAP1 from entering the nucleus, thereby preventing the transcription of pro-growth and anti-apoptotic genes (Zanconato et al. 2016). As one would expect, AmotL1 is frequently lost

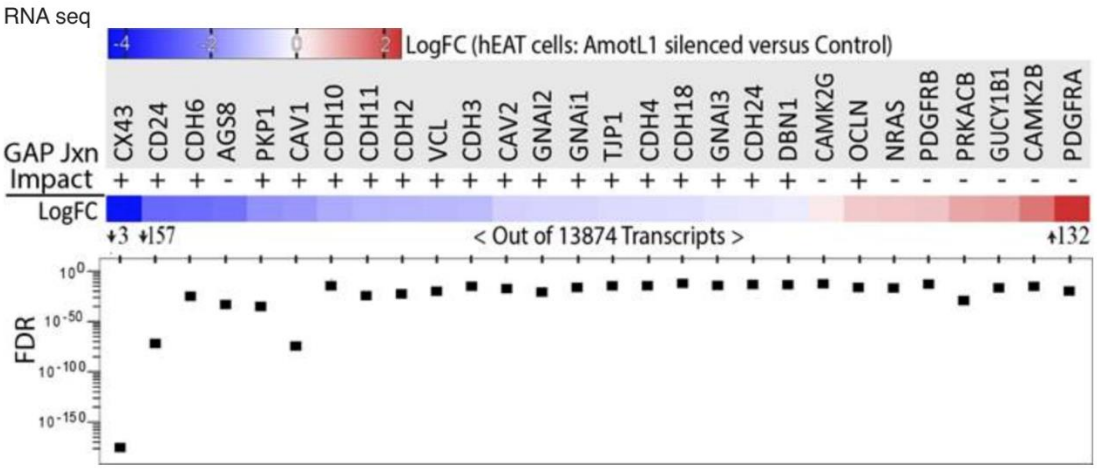

Figure 1: RNA-seq analysis of AmotL1-silenced hEAT cells. Shown across the heat map are gap junction transcripts identified from online databases that present the most differential expression upon RNAi against AmotL1. Most notable is the significant downregulation Cx43 mRNA. I did not conduct this analysis, nor did I create this figure, but it played a major role in establishing the direction of my research.

in these cancers. Follow-up cell-based studies reveal that AmotL1 silencing results in offering the growth advantages that are associated with tumorigenesis (Huang et al. 2018). A subsequent step into this investigation was to identify any other genes or transcripts that are differentially expressed because of the absence of AmotL1.

Using immortalized human embryonic astrocytes (hEATs), the laboratory silenced AmotL1 through lentiviral RNA interference (RNAi) and conducted RNA-seq on purified lysates prior to my admission. This analysis revealed drastic changes on transcript expression in a number of gap junction proteins. Remarkably, connexin-43 (Cx43) mRNA was downregulated, with a nearly 16-fold decrease relative to control cells (see Figure 1). Because Cx43 is essential for inter-astrocytic connections that are essential features in astrocyte differentiation, the loss of Cx43 is predicted to be a major event in cellular de-differentiation. For this reason, I sought to determine how a loss of Cx43 upon silencing of AmotL1 may promote cancer phenotypes.

An Overview of Cx43 and Gap Junctions

Cells transmit small molecules between each other to relay information by Gap Junction Intercellular Communication (GJIC), to share metabolites or to offload toxic materials. Cell-cell contacts at gap junctions offer cells the opportunity to exchange signals directly between their cytoplasm. Astrocytes, as support cells in the brain, rely heavily on gap junctions as their primary sites of intercellular contact and to carry out their core functions of transferring nutrients, absorbing toxic materials and relaying signals. Specifically, gap junctions allow the free diffusion of small molecules and ions, under one kilodalton in size, from one cell to another through narrow, water-filled channels contained within gap junctions (Beyer et al. 2019, Mayor 2015, Lathia et al. 2015, Laird 2006). Gap junctions themselves are specialized structures composed of a network of connexins (Beyer et al. 2019). These polypeptides are a highly diverse family of twenty-one known gap junction proteins, ranging in size from 23 to 62 kDa and named accordingly. Despite their differences, connexins all have highly conserved structures.

Connexins fold into four-pass transmembrane proteins with cytoplasmic N- and C-termini, two extracellular loops, and one intracellular loop (See Figure 2, Kotini and Mayor 2015, Laird 2006). Connexin monomers have a high affinity for oligomerization before arriving at the plasma membrane. It has been suggested that these polypeptides begin their association upon folding within the endoplasmic reticulum and continue progressively throughout the trans-Golgi network (Laird 2006). Six individual connexins oligomerize to form hexameric cylindrical structures known as hemichannels, or connexons. These complexes operate as pores in the membrane that can be selectively opened or closed by cellular stimuli, allowing for molecular transport into or out of a cell dependent of the

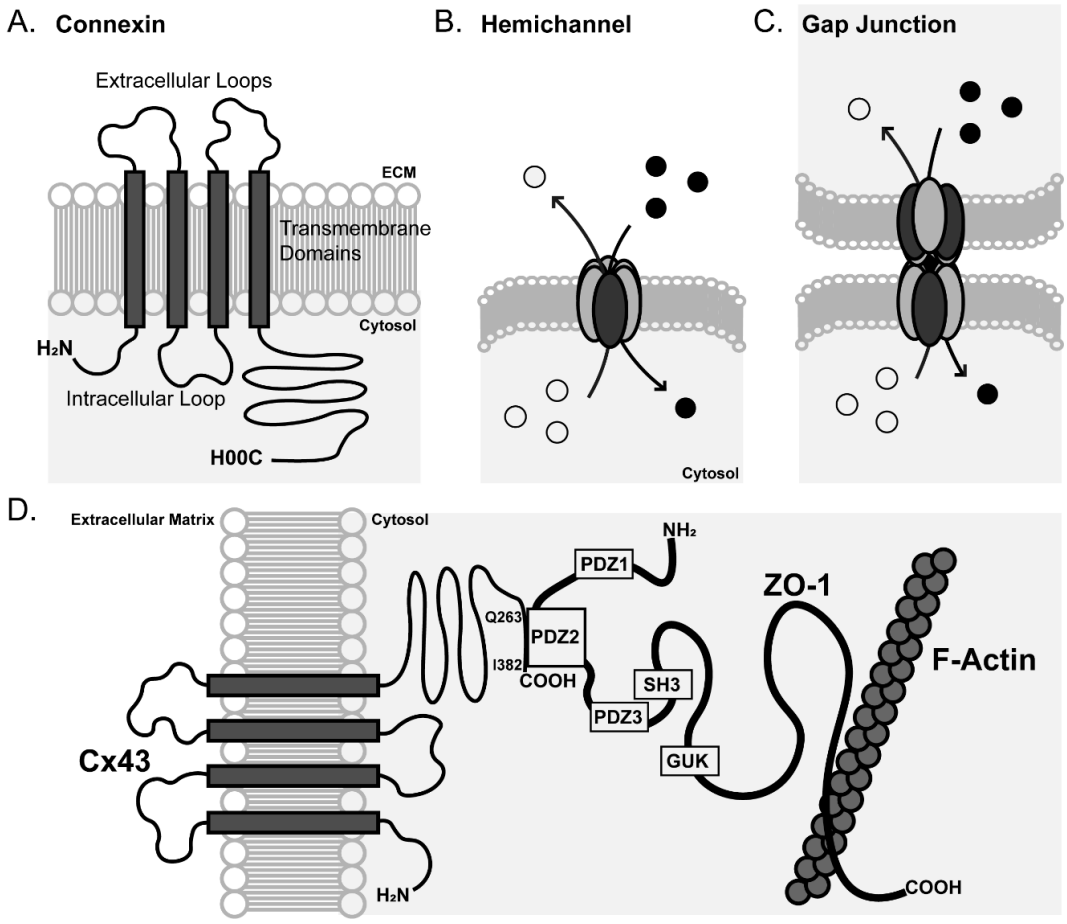

Figure 2: Formation of cellular gap junctions and functional interactions between Cx43, ZO-1 and F-actin. **A.** Generalized structure of a connexin protein. Each connexin has four transmembrane domains, two extracellular loops, one intracellular loop and cytoplasmic N- and C-termini. **B.** Formation of a hemichannel, or connexon. Six connexin proteins can oligomerize to form a hexameric structure, known as a hemichannel. These complexes connects the inside of a cell to the extracellular matrix (ECM) and allow for the import or export of small molecules and ions. **C.** Formation of a gap junction. Two hemichannels from adjacent cells can align and dock to one another, forming a gap junction channel. This gap junction directly connects the cytosol of two cells and allows for direct cell-cell communication through molecular transport. **D.** Interactions between the carboxyl-terminal tail of Cx43 and the second PDZ domain of ZO-1. ZO-1 serves as an actin-binding protein, linking the actin cytoskeleton to Cx43 and the plasma membrane through its proline-rich carboxyl-terminal tail. Adapted from illustrations by Laird (2006), Wu and Wang (2019).

context (Yin et al. 2018). In addition to channel opening and closure, cells can regulate

their GJIC by changing the expression of connexins. This can be achieved in a variety of ways: the alteration of transcription of connexin genes, such as *GJA1* that encodes Cx43, changing the rates of connexin protein degradation and assembly or by influencing factors associated with any of these processes (Laird 2006).

Single hemichannels allow for the molecular transport between a cell's cytoplasm and the surrounding extracellular matrix (ECM); whereas, two opposing hemichannels from adjacent cells can align end-to-end and bind to form a complete gap junction. This effectively connects their cytosols and allows direct cell-cell communication. Docking is achieved through the formation of disulfide bonds between cysteine residues found in the extracellular loops of each connexin subunit of a hemichannel (Kotini and Mayor 2015). Although single gap junctions can form and become active, plaques are frequently observed between cells, appearing as a punctate assemblies of multiple gap junctions (Bukasukas et al. 2000). Pulse-chase experiments have identified that newly-formed Cx43-based gap junctions form on the outside of these plaques and that older junctions are localized to the centers where they undergo internalization and eventual degradation by either, or both, the lysosome and 26S proteasome (Gaietta et al. 2002, Laing and Breyer 1995, Leithe and Rivedal 2004, Laing et al. 1997). Connexins themselves, even as constituents of oligomers, have short half-lives of only several hours before they are degraded. As mentioned, this is likely due to the physiological pressures and necessities in GJIC that face the cell (Laird 2006).

Cx43 is the most abundant connexin isoform in the central nervous system and is amongst the most studied in cancer; thus, the results from RNA-seq analysis showing a loss of Cx43 was speculated to be highly important for changes in cellular behavior (see

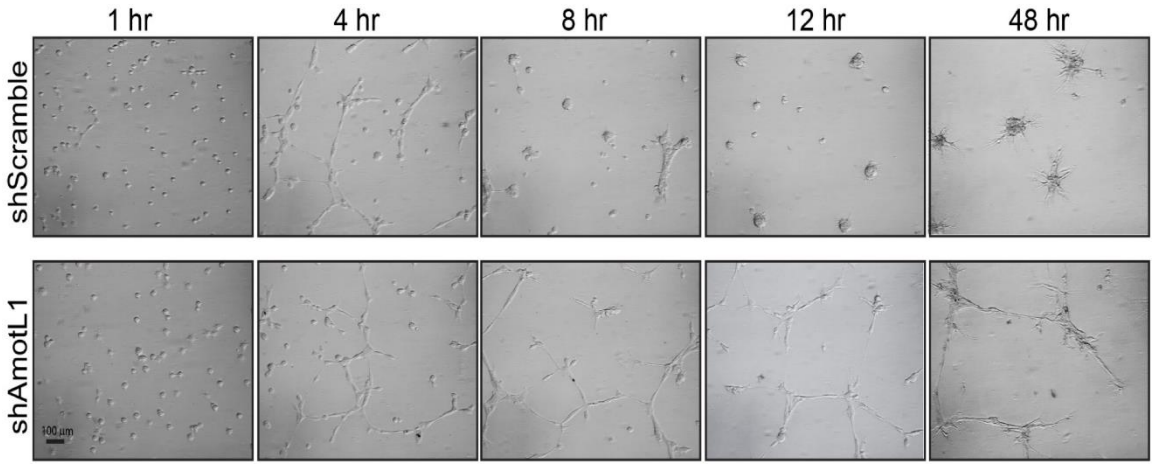

Figure 3: AmotL1 knockdown changes morphology in A172 human GBM cell lines. Provided are images of A172 cell growth in a three-dimensional Matrigel matrix at various time points. (Bottom) Cells infected with a lentivirus producing shRNAs against AmotL1. These cells experience a knockdown of AmotL1 through RNAi (Western blot analysis unavailable). (Top) Infected cells producing a negative control Scramble shRNA. At extended time points (12 hr, 48 hr), AmotL1-knockdown cells appear elongated and mesenchymal, suggestive of an invasive morphology. Control cells remain dendritic in their morphology. These images were taken by the Wells lab prior to my admission; I did not generate this figure.

Figure 1). I therefore sought to understand the impact of reduced AmotL1 on Cx43 localization in astrocytes. The expectation was that reduced Cx43 protein would inhibit gap junction formation and thereby reduce GJIC. Without GJIC, astrocytes lose cues that guide cellular polarity, and may ultimately assume invasive mesenchymal morphologies. Using AmotL1-silenced cells, I sought to define key mechanistic elements for the regulation of Cx43 that could, in turn, explain the proximal mechanisms that eventually drive the malignant phenotypes observed in the progression of GBM.

Tumor-Suppressive Roles of Cx43 in Carcinogenesis

Throughout the literature there has been extensive speculation of the putative roles of Cx43 loss in cancer. It is established that GJIC is commonly lost in both dividing and cancer cells, due to changes in connexin expression and cellular localization (Wu 2019).

Downregulation of Cx43, both at the transcript and protein level, has also been shown to lead to a loss of gap junction formation. Likewise, a re-localization of Cx43 from cortical membranes to cytoplasmic compartments reduces the formation of gap junctions and lowers the overall amount of GJIC. However, Cx43 has been shown to demonstrate both tumor-suppressive and oncogenic functions.

Many connexins at the cellular cortex, including Cx43, can bind β-catenin to reduce the amount of β-catenin available for nuclear translocation within the Wnt signaling pathway (Spagnol *et al.* 2018, Dianati et al. 2016). In normal cells, the Wnt signaling pathway is required for cell growth and proliferation (Komiya and Habas 2008). Wnt stimulatory factors act as ligands to bind the Frizzled receptor on the plasma membrane, leading to the cytoplasmic phosphorylation of the lipoprotein receptor-related protein (LRP). This active LRP binds to a multi-protein complex containing β-catenin, preventing the ubiquitination of β-catenin by β-TrCP and subsequent proteasomal degradation. β-catenin is then free to translocate into the nucleus and displace the Groucho inhibitor from the TCF transcription factor (Macdonald et al. 2009). This permits the transcription of genes that promote growth and proliferation. Therefore, the binding between Cx43 and β-catenin produces tumor suppressive effects by inhibiting Wnt signaling including: decreased growth, proliferation and reduced expression of Bcl-2 anti-apoptotic regulators, resulting in increased cell death (Polakis 2012).

Overexpression of Cx43 in LH7 lung cancer and HT29 colon cancer cells results in reduced proliferation of both cancer types (Sirnes et al. 2012, Xu et al. 2008). Thus, reduced levels of Cx43 upon a loss of AmotL1 proteins is predicted to have oncogenic effects. In part, this may occur via the freeing of β-catenin to stimulate expression of Wnt target genes.

For instance, increased expression of the antiapoptotic Bcl-2 regulator would increase the rate of cellular proliferation and inhibit apoptosis (Campbell and Tait 2018). In addition to inhibiting β-catenin, Cx43 may inhibit cancer by playing a pivotal role in establishing cell polarity. In both breast cancer and glioma cells, overexpression of Cx43 shifts cells from a mesenchymal to epithelial phenotypes (Lin et al. 2002, McLachlan et al. 2006). This supports my prediction that a loss of Cx43 may lead to mesenchymal morphologies in astrocytes and potentially increased invasiveness.

Cx43-containing gap junctions promote polarity by mediating cell-cell cohesion through their extracellular cysteine residues as well as adhesion to ECM (Wu 2019). Downregulation of Cx43 reduces GJIC in U251 glioma cells and leads to increased motility in a wound-healing assay. However, Cx43 downregulation impairs invasion in a transwell assay (Strale et al. 2011). Upon expression of exogenous connexin proteins, glioma cells have demonstrated increased adhesiveness to extracellular surfaces in vitro (Lin et al. 2002). These observations suggest that a loss of Cx43 would lead to both reduced GJIC and cohesion, events that are both associated with invasive phenotypes characteristic of metastatic cells.

Evidence also supports a tumor-promoting role for Cx43 in gastric, prostate and melanoma tumors that have increased levels of Cx43 mRNA and protein. The consequent increased cohesion between cancer cells and healthy cells as well as enhanced GJIC, promotes migration and invasion in vitro (Lamiche et al. 2011). Similar observations have been made in C6, GL15 and 8-MG glioma cells (Oliveira et al. 2005). Since Cx43 function in carcinogenesis is likely to be cell-specific, a deeper investigation in this human

embryonic astrocyte system is warranted to understand the impact of its loss upon AmotL1 suppression.

ZO-1 as a Cx43- and Actin-Binding Partner

Due to the difficulties of imaging Cx43, even following antibody optimization and different cell-culturing conditions, the tight junction protein zona occludens-1 (ZO-1) was imaged to ascertain the degree of cell-cell contacts. ZO-1 is a 220 kDa scaffolding protein that contains several domains supporting protein-protein interactions, including three PDZ domains, a Src-homology 3 (SH3) domain, and a guanylate kinase homology domain (GUK) (see Figure 2; Giepmans and Moolenaar 1998, Laing et al. 2005). As a peripheral membrane protein, it binds directly to both the actin cytoskeleton, through its proline-rich C-terminus, and junctional proteins present in the plasma membrane, including Cx43. Structural and functional mutation studies have shown that the second PDZ domain of ZO-1 binds the C-terminus of Cx43 between amino acids Q263 to the terminal I382 (Sorgen *et al*. 2004).

Previous work from others finds prominent colocalization of ZO-1 and Cx43 (Giepmans and Moolenaar 1998). However, ZO-1 is mainly detectable at the cellular peripheries and particularly at cell-cell contacts, unlike Cx43 which is found predominantly in the cell interior. ZO-1 localization therefore marks cell-cell contacts and is a marker of cytoskeletal changes responsible for establishing cellular polarity, morphology and direction in migration.

Actin Dynamics in Guiding Cellular Polarity

The actin cytoskeleton is a complex network of interlinking proteins that extend throughout the cell. Actin networks dictate the cellular architecture required for division, motility,

differentiation and polarity (Smyth et al. 2012, Tojkander et al. 2012). Often, abnormalities in the actin cytoskeleton or related proteins lead to the development of serious pathologies, including cancer. Actin filaments are polymers of actin, a highly globular 42 kDa protein that possesses inherent ATPase activity that increases upon polymerization. In the presence of high ATP levels, colliding monomers form a nucleus that undergoes elongation to form filamentous F-actin. Actin filaments themselves have polarity at their two distinct ends: a barbed (+) end that quickly accepts ATP-bound G-actin monomers for filament growth, and a pointed (-) end that is slow-growing. Actin filaments, as individual 8 nm thick strands, are weak and can easily be broken by mechanical forces; however, they can form much more stable complexes when bundled and cross-linked by actin-binding proteins.

Actin stress fibers are dynamic, antiparallel bundles of actin filaments that are crosslinked by proteins such as α-actinin and filamin (Tojkander et al. 2012). Present in both motile and non-motile cells, stress-fibers serve critical roles in providing the contractility forces required for migration, morphogenesis and cellular adhesion. Frequently, stress fibers are anchored to focal adhesions, which are adhesive points of contact between the actin cytoskeleton and ECM, often found near the cell body. In migrating cells, new stress fibers and focal adhesions form towards the leading edge and provide adhesion to new surfaces. As this occurs, myosin-mediated contractions and the degradation of actin filaments in the trailing edge results in a loss of adhesion, allowing the cell to release from the ECM and move with the leading edge. Both focal adhesions and stress fibers have become of interest in understanding the observations that I have routinely made.

A consistent shift in astrocyte morphology upon knockdown of AmotL1 through RNAi is observed in which cells become more flattened and therefore occupy a greater cross-sectional area compared to controls. However, counter to expectations, AmotL1 knockdown results in a loss of both stress fibers and focally-localized actin (See Figure 8). Instead, cortical actin is increased as is the distribution of ZO-1 to the cellular cortex. This matches the changes that promote polarity in intestinal epithelial cells. Upon activation and translocation of the LKB1 serine/threonine kinase to the cytoplasm following induction of STRAD, ZO-1 redistributes to the cell cortex (Baas et al. 2004). This is in response to actin cytoskeletal remodeling to form brush borders, a highly absorptive array of microvilli that cover the apical surfaces of intestinal cells. Considering cells grown on rigid surfaces develop more prominent stress fibers, my results are puzzling (Prager-Khoutorsky et al. 2011). It is important to note that AmotL1-silenced cells retain adhesion to the ECM in vitro. The potential mechanisms and implication of this cytoskeletal rearrangement in the context of GBM is further discussed in the *Results and Discussion*.

Methods

Cell Culture

Normal human embryonic astrocytes (hEAT) were grown in Dulbecco's Modified Eagle's Medium (DMEM) (HyClone™, Logan, UT) supplemented with 10% fetal bovine serum (FBS, Biowest, Cat No: S1620), 1% Penicillin Streptomycin (5 mL at 100x; Gibcom™, REF: 10378-016), 0.0001% hydrocortisone, 0.0005% insulin, and 0.001% N-acetylcysteine. Human glioblastoma (A-172) cells (American Type Culture Collection, Manassas, VA, A-172 [A172] (ATCC® CRL-1620™)) were grown in DMEM (HyClone™, Logan, UT) supplemented with 10% fetal bovine serum (FBS), 1% Penicillin-Streptomycin. Transfectable human embryonic kidney cells (HEK293) were utilized for lentiviral production (293T (ATCC® CRL-3216™)). These were grown in DMEM (HyClone™, Logan, UT) supplemented with 10% FBS and 1% Penicillin-Streptomycin. All cells were maintained at 37ºC with 5% CO_2. Lentiviral-infected cell lines were cultured in each cell type's respective complete media. To aid in adhesion, all hEAT cells were grown on collagen-coated plates. To induce differentiation, cells were seeded in plates and grown in 50% Barris Neurobasal® Medium supplemented with 1% Penicillin-Streptomycin, 1% SATO medium, 0.001% N-acetylcysteine and 0.001% HBEGF for 60 hours prior to collection.

Bacterial Transformation and Plasmid Isolation

Escherichia coli cell cultures were exposed to ampicillin-resistance-encoding plasmid constructs (pRRE, pVSV-G, pRSV-rev, and lentiviral: shAmotL1, shScramble, control-YFP, AmotL1 WT-YFP, AmotL1 262D-YFP, AmotL1 262A-YFP, AIP4-mCherry, Nedd4-1-CFP) prior to heat-shock treatment for cell competency and DNA uptake. After

a 1 hour recovery incubation in Luria broth (LB), cells were plated onto LB agar plates with ampicillin and incubated at 37 ^{o}C overnight. The following day, isolated colonies were transferred to sterile flasks containing (1x) Yeast Extract Tryptone liquid microbial growth media and ampicillin. Beakers were placed on an orbital shaker overnight (250 rpm) at room temperature. After 16 hours, cell solutions were transferred to bottles for a 10-minute centrifugation at 6300 rpms. Supernatant was removed and cells were vortexed with a buffer enabling RNA hydrolysis upon lysis (50 mM Tris-Cl pH 8.0, 10 mM EDTA, 100 ug/ml RNAse A). Once resuspended, cells were lysed using a detergent-containing buffer (200 mM NaOH, 1% SDS). Cells were exposed to a third buffer (3M potassium acetate and glacial acetic acid) that promotes macromolecular renaturation. Centrifugation was repeated under the same conditions and supernatant was filtered. Anion-exchange column chromatography was utilized to purify DNA. These samples were mixed with isopropanol and centrifuged at 13000 rpms for 10 minutes at 4 ^{o}C. Pelleted DNA was isolated, dried with 70% ethanol and resuspended in Tris-EDTA (TE) buffer.

DNA Quantification

DNA concentration and purity were quantified using an ND-1000 spectrophotometer V3.8.1 (NanoDrop®). Stock plasmid solutions were diluted to 500 ng/μL in TE for use in *transfection.*

Transfection of Transforming Cells

Healthy 293T cells were plated onto 10 cm plates in complete media outlined above and incubated at 37^{o}C with 5% CO_2 for 24 hours prior to transfection. In polysterene tubes, 6 μg of pVSV-G, 5 μg of pRSV-rev and 10 μg of pRRE was added to serum-free DMEM as well as 20 μg of desired lentiviral DNA. While vortexing, 25 μL of polyethyleneimine

was added dropwise to each transfection mixture and left to incubate for 5 minutes at room temperature. Transfection mixtures were distributed evenly across each plate. After 4-18 hour incubation at 37ºC with 5% CO_2, transfection media was replaced plates with 7 mL of fresh DMEM. Cells were left to incubate overnight at 37ºC with 5% CO_2. The following day, infection media was collected off each plate and stored at 4 ºC ($t_{1/2}$ = 2 weeks).

Target Cell Infection

For RNAi experiments, target cells (control hEAT, hEAT Cx43 Untagged, A172) were seeded at 500,000 cells per 10 cm plate and left to incubate 12-24 hours at 37ºC with 5% CO_2 prior to infection. After lentiviral media was collected following transfection of 293T cells, 1.95 mL solutions made up of 0.65 mL viral media and 1.3 mL complete media (1:4) were created and added to target cells. An additional 40 µL of polybrene were added to each plate and tilted to distribute evenly. To achieve RNAi, AmotL1 shRNA lentiviral vectors and shScramble negative control shRNA lentiviral vectors were synthesized prior to my entry into the Wells lab. The RNAi efficiency of AmotL1 shRNA was determined using Western blot. In later experiments looking at cytoskeletal dynamics under conditions with AmotL1 Control, AmotL1 WT, AmotL1 262D, AmotL1 262A +/- AIP4 or Nedd4-1, cells were seeded onto 6 cm plates at 200,000 cells/plate and incubated for 24 hours prior to infection. Cells were infected with 1 mL of virus (diluted 1:5 in media) at hours 24 and 28 and media was replaced at hour 32. After an additional 24 hours of growth, cells were seeded onto coverslips and incubated at 37ºC with 5% CO_2 for 48 hours before fixation.

Western Blot Analysis

Protein concentrations were evaluated using the bicinchoninic acid assay (Thermo Scientific™, Pierce™ BCA Protein Assay Kit). 25-30 µg of each lysate extract was

separated on 8% or 10% SDS polyacrylamide gels using electrophoresis at 160 Volts. The gel-separated proteins were transferred onto a nitrocellulose membrane using an orthogonal charge set to 24 V for 55 minutes. After blocking membranes with 5% non-fat milk powder solution overnight at 4^{o}C, or on a rotator at room temperature for 20 minutes, membranes were probed using the following primary antibodies: overnight on nutator at 4^{o}C with rabbit-antihuman GAP-DH (1:1000), mouse-antihuman Cx43 (1:1000), mouse-antihuman β-tubulin (1:2000), or 2 hours with rabbit-antihuman AmotL1 (1:2000). The membranes were washed and incubated with secondary antibody for 30 minutes in dark on a rotator. Secondary antibodies include: goat anti-rabbit IRDye® 680 (1:20,000; Odyssey, 827-08367), goat anti-mouse IRDye® 800CW (1:20,000; Odyssey, 827-08364). Membranes were analyzed using an Odyssey infrared imager (Li-Cor, USA). ImageJ software was used to quantify protein band intensities.

Immunofluorescence

Cells were plated onto acid-washed cover slips to improve adhesion. Media was removed after incubation and cells were washed twice with 1xPBS. They were fixed by incubating with 4% paraformaldehyde for 10 minutes. Fixed cells were washed twice and incubated for 30 minutes with blocking buffer (1xPBS supplemented with 5% bovine serum albumin (BSA), 0.002% saponin, and 100% 1000x NaN_3 for bacterial and fungal inhibition). After incubation, cells were washed once and incubated for 1 hour at room temperature with antihuman monoclonal Cx43 Ab (1:400; Santa Cruz Biotechnology, sc-59949), polyclonal Cx43 Ab (1:400), monoclonal ZO-1 (1:1000), polyclonal AmotL1 (1:1500, made in house), monoclonal Arf6 (1:500; Santa Cruz Biotechnology, sc- 7971), monoclonal β-tubulin (1:1000; Developmental Studies Hybridoma Bank, AA4.3, AB_579793), or

monoclonal LAMP1 (1:400; Developmental Studies Hybridoma Bank, 1D4B, AB-528127). After two washes, cells were incubated with secondary antibodies conjugated with AlexaFluor-488 (1:1000; Abcam), AlexaFluor-594 (1:1000; Santa Cruz), or phalloidin (1:3000; Santa Cruz, sc-363795) for 25 minutes. Afterwards, cells were washed twice. For nuclear staining, cells were incubated for 1 minute with 750 mL Hoechst solution (1:1000; 10 mg/mL). Coverslips were washed twice more in (1x) PBS and in deionized water before fixation to slides. Images and observations were performed using a Zeiss fluorescent microscope and AxioVision 4.8 software. Exposure times varied by antibody across treatments.

Optimization of Primary Antibodies for Use in Immunofluorescence

Prior to any experimental conditions, primary antibodies were applied to fixed cells at various dilutions to optimize staining and avoid the overuse of supplies. Attempted dilutions of each antibody are provided in parentheses and include: monoclonal Cx43 (1:200, 1:400, 1:600), polyclonal Cx43 (1:200, 1:400, 1:600), monoclonal ZO-1 (1:600, 1:800, 1:1000), polyclonal AmotL1 (1:250, 1:500, 1:750, 1:1000, 1:1500), monoclonal β-tubulin (1:500, 1:1000), monoclonal Arf6 (1:500, 1:1000), monoclonal Lamp1 (1:200, 1:400) and phalloidin (1:1000, 1:500, 1:2000, 1:2500, 1:3000). Images for each antibody dilution are included in Appendix A.

Image Processing in AxioVision

After capturing images in AxioVision 4.8, each was processed for optimal viewing conditions. Images captured using a Z-stack received a *Z-stack Correction* under the *Processing* and *Adjust* tabs, in which the parameters *Correct Decay*, *Correct Flicker*, and *Correct Background* were set to *True*. All images had *Unsharp Masking* applied to them

using the *Sharpen* feature. The parameters for *Unsharp Masking* were set as follows: *Color Mode* – RGB; *Radius* – 2; *Strength* – 1; *Level Low* – 0; *Level High* – 100; *Threshold Mode* – Binary; *Auto Contrast* – No; *Auto Contrast Tolerance* – 5; *Clip To Valid Bits* – Yes. Prior to export and Adobe editing, images could be optimized using the *Brightness/Contrast/Gamma* settings.

Results and Discussion

Knockdown of AmotL1 reduces Cx43 protein expression yet causes an increase in its distribution to cell-cell contacts at potential gap junctions.

Normal hEAT cells have low levels of Cx43 protein that are detectable by Western blot analysis. Therefore, an initial goal was to generate a cell line that stably overexpresses Cx43. According to RNA-seq data (Figure 1), a knockdown of AmotL1 is anticipated to result in a loss of Cx43 mRNA; I predicted that this would correlate with a reduction in Cx43 protein. Thus, to quantify global changes in Cx43 protein expression and to observe changes in Cx43 localization upon RNAi against AmotL1, I felt that it was essential to use a cell line that would not experience a *complete* loss of Cx43 protein. Shown below in Figure 4, I successfully generated a Cx43-overexpressing cell line via lentiviral infection, which I refer to as hEAT Cx43 Untagged throughout this thesis. With these cells, I sought to determine the effects of AmotL1 knockdown on Cx43.

Small inhibitory RNA (RNAi) has become a highly-utilized technique that introduces double-stranded RNA molecules to target a particular host mRNA for degradation and consequent loss of expression (Kang et al. 2009, Walgren and Mcleod 2005). The Wells laboratory has designed lentiviruses encoding short hairpin (sh) RNAs designed against the mRNA transcripts encoding AmotL1 or a negative control "Scramble" sequence, which would identify any potential effects of the infection process itself. Once target cells are infected, the virus incorporates itself into the host genome and begins both

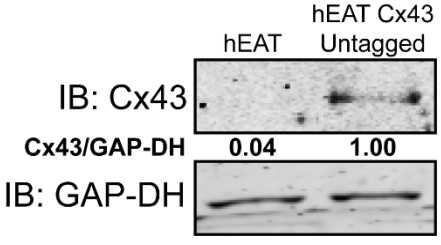

Figure 4: Overexpression of Cx43 protein by hEAT Cx43 Untagged cell lines. Western blot analysis reveals a 25-fold increase in Cx43 protein in hEAT Cx43 Untagged cells relative to control hEAT cells.

replication and transcription of viral shRNA transcripts. As these double-stranded shRNAs are produced and released into the cytoplasm, the endoribonuclease Dicer soon cleaves them into small-interfering (si) RNA molecules of about 21-23 nucleotides in length. Upon facilitated activation by Dicer, the RNA-induced silencing complex (RISC) component, Argonaute or *Slicer*, incorporates an unwound single-stranded siRNA as a guide strand while degrading the complementary passenger strand (Hammond 2005). RISC utilizes this guide strand to identify and specifically bind a target mRNA transcript via complementary base pairing. Once bound, Argonaute is activated and cleaves the host mRNA transcript; thereby preventing gene expression and protein translation (Ambesajir et al. 2012, Kim and Rossi 2008).

hEAT Cx43 Untagged cells were transduced with lentiviral RNAi against AmotL1. Western blot analysis validated the overexpression of Cx43 versus control cells (Figure 5B-C). As shown in the immunoblot, AmotL1 knockdown resulted in a significant reduction (~70%) in AmotL1 protein thus validating the efficiency of knockdown. Consistent with RNA-seq data conducted previously by the Wells laboratory (Figure 1 in the *Introduction*), a loss of AmotL1 is accompanied by a significant reduction (~90%) in Cx43 protein expression (Figure 5C). Cx43 and AmotL1 levels were normalized to either GAP-DH and β-Tubulin controls, respectively. I then sought to validate my prediction that a reduction in Cx43 would result in less Cx43 at cell-cell junctions.

After growing cells on acid-washed coverslips for 60 hours, nuclei were stained with Hoechst dye, a polyclonal Cx43 antibody with emission at 594 nm, and a monoclonal ZO-1 antibody with emission at 488 nm. As discussed in the *Introduction*, ZO-1 was used to mark cell peripheries and to look for colocalization with Cx43 at gap junctions. I

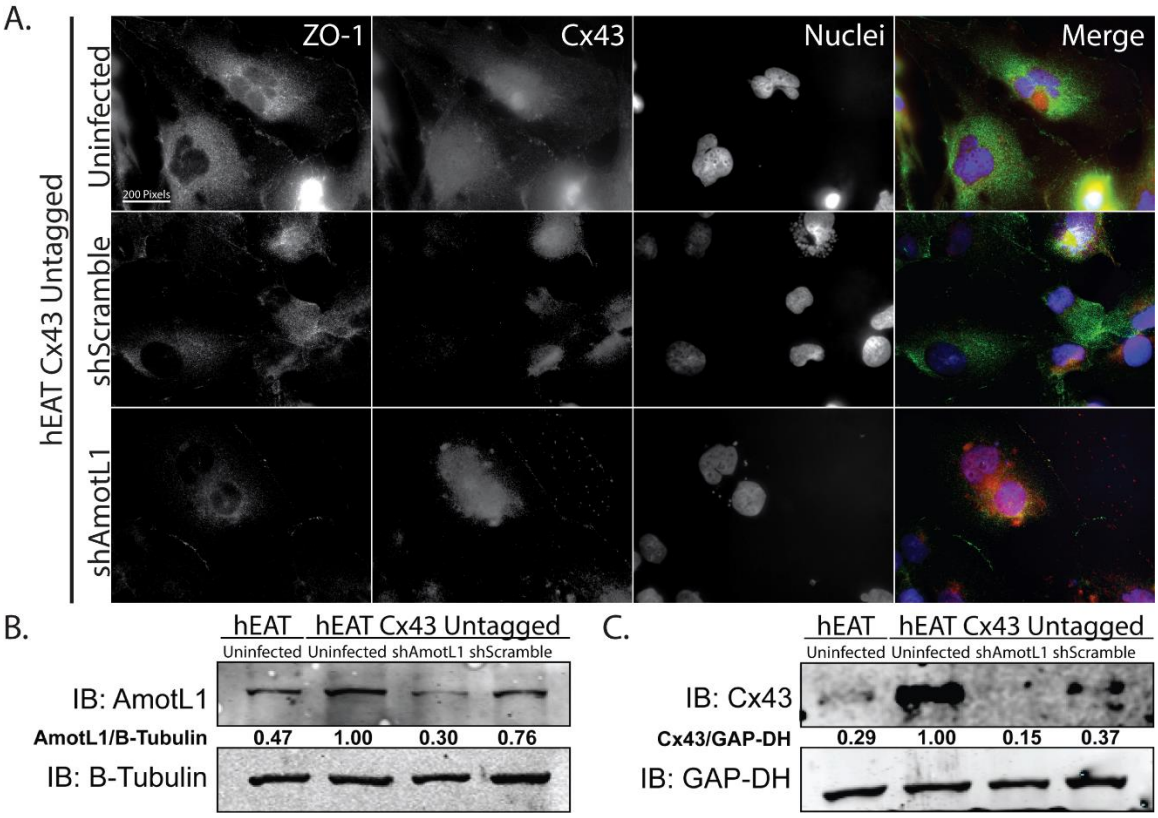

Figure 5: AmotL1 knockdown through RNAi causes a reduction in Cx43 expression but increases Cx43 localization to cellular junctions**. A.** Localization of Cx43 and ZO-1 in hEAT Cx43 Untagged cells by lentiviral treatment. Upon shAmotL1 RNAi, the relative concentration of Cx43 to cell-cell contacts and peripheries increase relative to control cells. **B.** Western blot analysis reveals a 70% knockdown of AmotL1 relative to uninfected hEAT Cx43 Untagged cells. **C.** Knockdown of AmotL1 results in an 85% reduction in Cx43 in hEAT Cx43 Untagged cells. Uninfected control hEAT cells are included to validate overexpression of Cx43 in hEAT Cx43 Untagged cells in this experiment.

predicted that a loss of Cx43 would result in reduced gap junction formation and cell-cell cohesion. These observations may support the mesenchymal morphologies and apparent invasiveness associated with AmotL1-knockdown astrocytes grown in three-dimensional culture (Figure 3). Remarkably, the opposite of my prediction of reduced Cx43 at junctions was observed.

Upon knockdown of AmotL1, there was a noticeable shift in the distribution of Cx43 from the cytosol to both the cell cortex, presumably for hemichannel formation, and to cell-cell contacts (Figure 5A). To validate this observation, nine microscopic fields from each treatment group were randomly selected for imaging based only on nuclei density and positioning. Healthy cells that made clear contacts with adjacent cells without stacking or climbing on top of one another were desired. Upon viewing the 488 nm and 594 channels, if a field revealed no cell-cell contacts or if the cells appeared to be physically damaged by the fixation procedure, a new field was randomly selected by nuclei once again. To reduce bias, images were anonymously labeled, shuffled and two weeks of time were allowed to pass before gap junctions were identified for quantification. Independent sites where both Cx43 and ZO-1 colocalized at cell-cell contacts were counted. To take into consideration the slight variations in cell densities between images, this number was divided by the total number of nuclei of adjoining cells present in the microscopic field. If a cell was not in contact with any other cell in the field, its nucleus was not included in this count.

I then calculated colocalization score ratios, abbreviated as CS, of ZO1-Cx43 colocalization sites at cell-cell contacts to the appropriate number of adjoining nuclei in each field (Table 1). When plotted into box and whisker plots, these scores present a trend. Shown in Figure 6, both normal hEAT and hEAT Cx43 Untagged cells treated with RNAi against AmotL1 experience increased colocalization compared to their respective control groups, uninfected or infection with shScramble-encoding lentivirus. Single-factor analysis of variance and post-hoc tests (not shown) indicate that shAmotL1-treated cells had a mean CS significantly higher than uninfected group in normal hEAT cells ($p<0.002$). In the Cx43-overexpressing cell line, there was no significant difference between uninfected

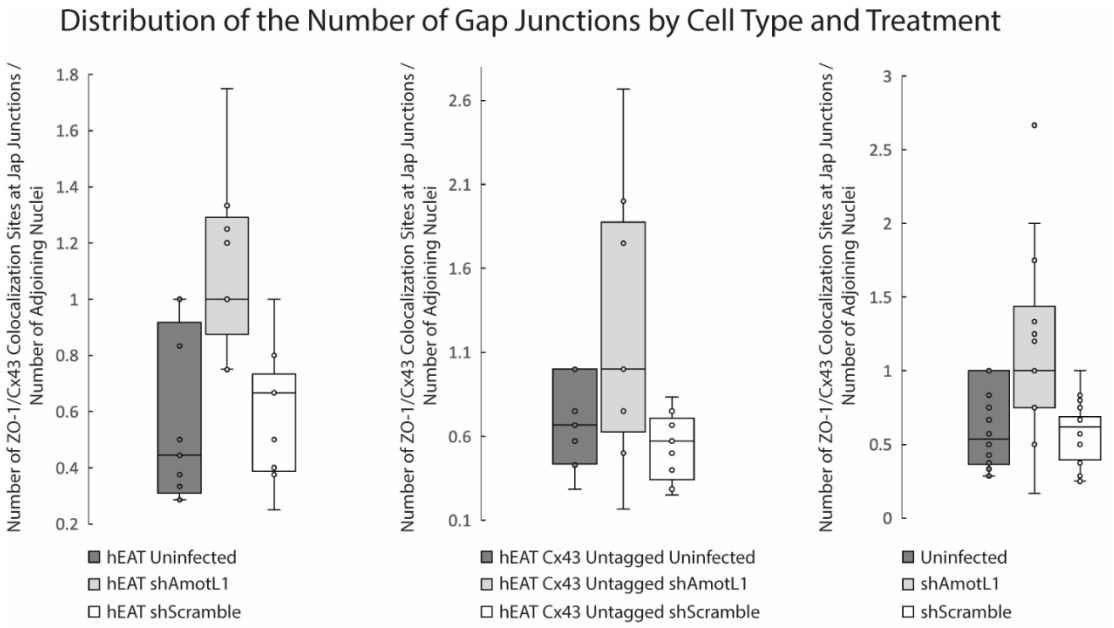

Figure 6: Quantification of Cx43–ZO-1 colocalization**. A**. Boxplots of colocalization scores, CS (CS = number of sites where there is colocalization of Cx43 and ZO-1 at cell-cell contacts : number of independent nuclei that are in adjoining cells within the field of vision). Both control hEAT cells and hEAT Cx43 Untagged cells experience greater colocalization of Cx43 and ZO-1 to junctions upon AmotL1 knockdown. N=9 fields per group.

cells and cells experiencing RNAi against AmotL1; however, the shScramble-treated cells had a significantly lower mean score compared to those treated with shAmotL1 (p=0.027). In the rightmost graph, cell types were condensed based on treatment (N=18 fields). It is clear that AmotL1 knockdown results in an increased distribution of Cx43 to cell-cell contacts as well as enhanced colocalization with ZO-1 at these sites. Taken together, these data suggest that AmotL1 plays a pivotal role in limiting gap junction formation. Despite the significant reduction in Cx43 protein expression, a knockdown of AmotL1 appears to increase the formation of gap junctions in human embryonic astrocytes. In many cases, well-defined gap junctions were observed in AmotL1-knockdown cells and appear as punctate structures running perpendicular to the plasma membrane at cell-cell contacts.

After extensive imaging and optimization, I felt that control hEAT cells expressing endogenous Cx43 present better gap junction formation compared to hEAT Cx43 Untagged cells. Therefore, only they are used for further analysis. In Appendix B, I have included multiple images for each cell type and treatment for comparison (Figures 13-15). Next, I sought to explore the effects of cellular differentiation on gap junction formation.

Embryonic hEAT cells exist in a naturally undifferentiated, pluripotent state. After lentiviral infection or not, cells were subjected to 60 hours of growth in Barris Neurobasal media (see *Cell Culture* in the *Methods*) before fixation. This conditioned media has an abundance of supplements including those of the B-27 category, a widely-used and trusted product in neuronal cell culture (ThermoFischer Scientific). Although the mechanism by which this media induces commitment is still unclear, it is believed that growth factors and other signaling molecules may function through pathways similar to TGFβ, Wnt, Hedgehog and insulin-like growth factor receptor pathways to stimulate terminal differentiation in embryonic astrocytes (Dhara and Stice 2008).

As previously observed, RNAi against AmotL1 leads to increases in the relative concentrations of Cx43 and ZO-1 at gap junctions, cell-cell contacts, and peripheries compared to control treatments. Remarkably, however, the addition of Barris neurobasal media stimulates extensive localization to junctions in cells across all treatments (Figure 7). These data suggest that a loss of AmotL1 may mimic or induce the effects of differentiation. It may also be that AmotL1 protein is lost in differentiated cells, leading to the increased formation of intercellular gap junctions despite reductions in Cx43 protein.

A.

Groups	Count	Sum	Average	Variance
hEAT Uninfected	9	5.05754	0.561948854	0.089362262
hEAT shAmotL1	9	10.03333	1.114814815	0.097808642
hEAT shScramble	9	5.325	0.591666667	0.054479167

Source of Variation	SS	df	MS	F	P-value
Between Groups	1.740683713	2	0.870341857	10.80498573	0.000450627
Within Groups	1.933200568	24	0.080550024		
Total	3.673884281	26			

B.

Groups	Count	Sum	Average	Variance
hEAT Cx43 Untagged Uninfected	9	6.146825	0.6829806	0.074768693
hEAT Cx43 Untagged shAmotL1	9	10.83333	1.203703704	0.621720679
hEAT Cx43 Untagged shScramble	9	4.92381	0.547089947	0.041591238

Source of Variation	SS	df	MS	F	P-value
Between Groups	2.162281338	2	1.081140669	4.394400773	0.02364985
Within Groups	5.904644887	24	0.24602687		
Total	8.066926225	26			

C.

Groups	Count	Sum	Average	Variance
Uninfected	18	11.20437	0.622464727	0.08111569
shAmotL1	18	20.86667	1.159259259	0.340693537
shScramble	18	10.24881	0.569378307	0.045735595

Source of Variation	SS	df	MS	F	P-value
Between Groups	3.833556457	2	1.916778229	12.29900198	4.37548E-05
Within Groups	7.948261964	51	0.155848274		
Total	11.78181842	53			

Table 1: Single-factor ANOVA statistical analysis of Cx43–ZO-1 colocalization scores, CS**. A.** Analysis of CS in control hEAT cells. Post-hoc tests (not included) reveal that the mean CS for hEAT shAmotL1-treated cells is significantly higher than that of the two control groups. **B.** Analysis of CS in hEAT Cx43 Untagged cells. hEAT Cx43 Untagged shAmotL1-treated cells have a mean CS that is statistically higher than that of the hEAT Cx43 Untagged shScramble-treated cells, but not that of uninfected cells. **C.** Analysis of CS in combined cell types (control hEAT and hEAT Cx43 Untagged) based solely on treatment alone. Post-hoc analysis reveals that a knockdown of AmotL1 results in statistically higher mean CS.

Ultimately, these observations were counterintuitive and I feel that further investigation will be warranted in the future to better understand these mechanisms. Consistently throughout these experiments, cell flattening is observed upon knockdown of AmotL1. This suggests that cytoskeletal components may be affected by the changing

levels of AmotL1 through RNAi. Taken together, I chose to investigate the effects of AmotL1 expression changes on cytoskeletal actin dynamics.

Future directions regarding Cx43

I had predicted that as Cx43 expression decreases following AmotL1 knockdown, cells would lose Cx43 at gap junctions and the associated intercellular communication; however, my observations regarding Cx43 localization to gap junctions were contradictory to these preconceived beliefs. It may prove insightful to further investigate the phenomena that has been observed. Unfortunately, I feared that this project would not yield satisfactory findings during my limited time in Indianapolis. It was therefore essential that I progress to other experiments for my Masters research.

As discussed, a significant shift in the distribution of Cx43 from the cytoplasm to the plasma membrane occurs upon knockdown of AmotL1. I hypothesize that this may be due to some inhibitory interaction that exists between Cx43 and AmotL1. It is possible that AmotL1 binds Cx43 and prevents its trafficking to the membrane. Upon RNAi against AmotL1, Cx43 may exist free of these interactions and be able to travel. To my knowledge there have not been any publications regarding the physical interaction between AmotL1 and Cx43. I would suggest co-immunoprecipitation assays be conducted to validate how these two proteins interact. By creating mutations in bait AmotL1 at a variety of sites and subjecting them to an abundance of prey Cx43 protein lysate, the residues on AmotL1 required for this interaction may be identified. An additional co-immunoprecipitation assay could be conducted in which Cx43 residues are mutated and exposed to purified AmotL1. Taken together, these experiments could potentially identify the domains specific amino-acid residues required for this protein-protein interaction to occur.

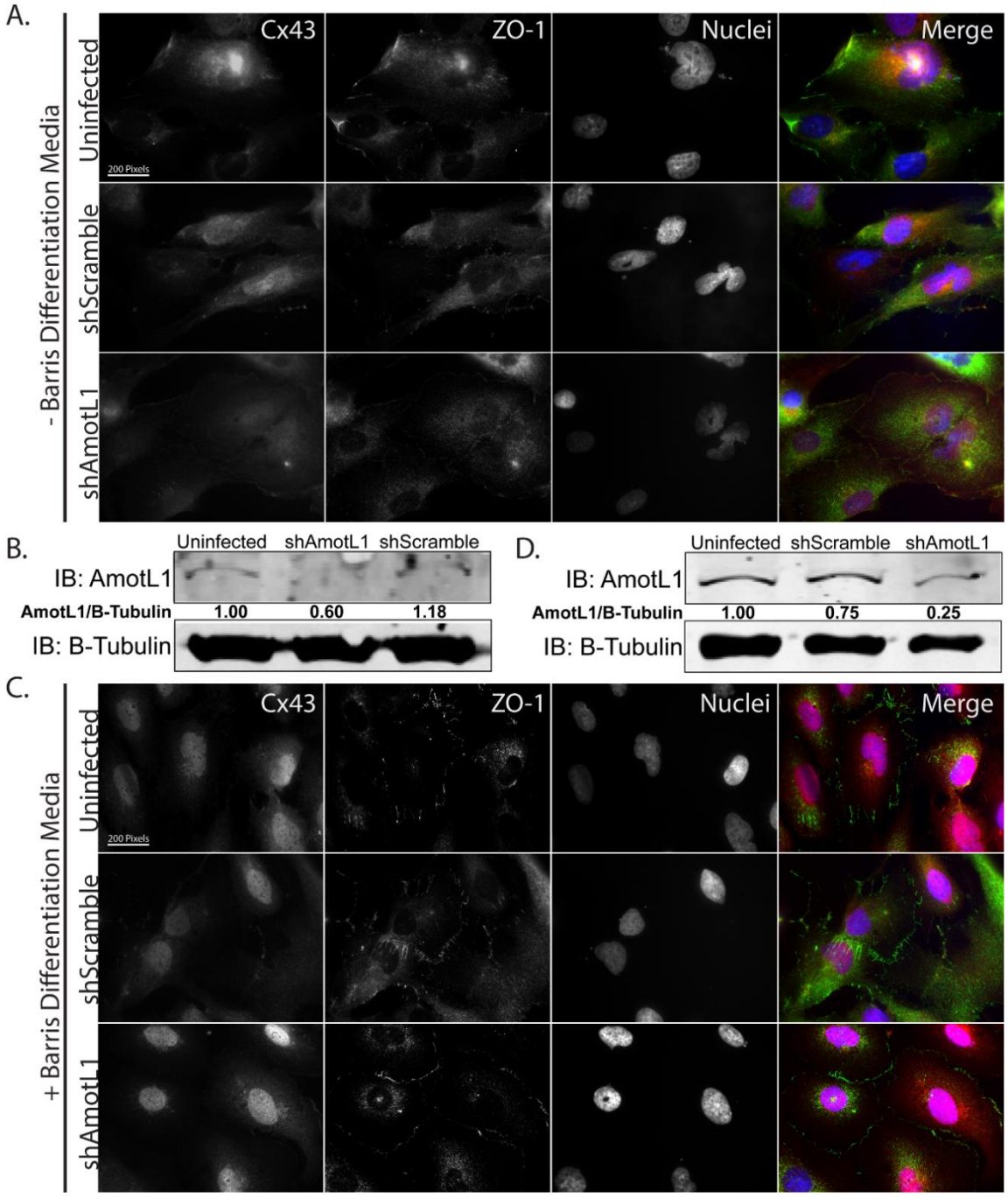

Figure 7: Cx43 and ZO-1 localization in undifferentiated and differentiated hEAT cells upon treatment. **A**. Cells grown in standard DMEM complete for hEATs. Upon knockdown of AmotL1, cells experience increased gap junction formation, suggested by the colocalization of Cx43 and ZO-1 to cell-cell contacts. **B.** Western blot analysis for cells shown in A, indicating successful AmotL1 knockdown via RNAi. **C.** Cells grown in Barris Neurobasal media. Differentiation increases gap junction formation and Cx43 localization to cell-cell contacts. **D.** Western blot analvsis for cells shown in C

Throughout the literature a majority of proteins bind the carboxyl-terminal domain of Cx43; however, this is because they interact with Cx43 when it is localized to the plasma membrane, often for scaffolding purposes. Throughout my imaging, I have observed an abundance of cytoplasmic Cx43, which may be interacting with AmotL1. Unfortunately, I was unable to stain both proteins simultaneously for immunofluorescent imaging since the Wells laboratory only possessed polyclonal antibodies against both. In the future, the lab could attempt to purchase and optimize a more specific monoclonal antibody for Cx43. Additionally, immunofluorescent imaging could be conducted on cells that produce a fluorescently-labeled AmotL1 or Cx43 protein. In later experiments, I generated hEAT cells labeled with a YFP-labelled AmotL1 that could be used for this purpose (see *Methods* for appropriate protocols).

I failed to explore the reasons for reduced Cx43 protein expression upon AmotL1 knockdown. There may be several reasons why cells experience this change. As may be supported by a co-immunoprecipitation assay, the binding of AmotL1 to Cx43 may serve as a protective mechanism prohibiting both the translocation of Cx43 and its degradation. The protein-protein interaction may prevent Cx43 trafficking to the lysosome or it may inhibit the ubiquitination of Cx43 by E3 ubiquitin ligases, thus protecting it from 26S proteasomal degradation. When cells experience RNAi and knockdown of AmotL1, Cx43 may lose this protective partner and experience the increased degradation as a potential explanation to the results seen in the Western blot of Figure 5C.

Consistent with the RNA-seq data (Figure 1), AmotL1 may influence the transcription of Cx43. It is known that AmotL1 regulates YAP/TAZ transcriptional co-activators and that a loss of AmotL1 allows these transcription factors to translocate into

the nucleus and induce expression of pro-growth, often oncogenic, genes (Chan et al. 2011, Zanconato et al. 2016). To explain the changes in Cx43 transcript levels seen in both patient sample data and in the AmotL1-silenced hEAT cells generated by the Wells laboratory, further investigation will be required. Although changes in Cx43 mRNA levels correlate with loss of AmotL1, connexin expression may be regulated by epigenetic mechanisms. Under consideration that 2-HG accumulates in lower grade gliomas and may promote secondary GBM, excessive hypermethylation of DNA may prevent expression of Cx43 (Oyamada et al. 2012).

Additionally, I did not conduct any functional assays to determine the effects of Cx43 localization to cell-cell contacts upon knockdown of AmotL1. Although the imaging revealed an increase in the formation of gap junctions upon both RNAi against AmotL1 and differentiation, a dye transfer assay could serve as a definitive measure of GJIC (Babica et al. 2016). Future experiments could generate an acceptor cell line that fluoresces an identifier protein. As mentioned, I have successfully expressed a YFP-labeled AmotL1 in hEAT cells which could serve this purpose in addition to its use in AmotL1-Cx43 colocalization studies. A fluorescent dye could then be added to a non-fluorescent donor cell population for uptake.

If using YFP-labelled AmotL1 in hEAT cells, Lucifer Yellow with emission at 594 nm may be an ideal dye. Once the donor cells appear to have received the dye, the two cell populations could be mixed evenly onto a new plate. After allowing a suitable time for the formation of gap junction (60 hours if seeding 200,000 cells of each population onto coverslips), cells could either be live-imaged or fixed for imaging. Using microscopy, the number of fluorescent acceptor cells that have taken in the dye could be quantified and

compared across the three treatment groups: uninfected, shScramble and shAmotL1. It is vital that the acceptor population be fluorescently labeled since fluorescence may be lost over time or incorporation by the lentivirus may not be completely efficient. If one were to add the fluorescent dye to fluorescent donor cells, these cells may lose their protein fluorescence without having transferred the dye to a non-fluorescent acceptor cell, giving the false illusion that an acceptor cell received dye from a donor through GJIC.

It may even be worthwhile to investigate the effects of changing AmotL1 levels on hemichannel activity. Upon both knockdown of AmotL1 and differentiation, astrocytes experience increases in Cx43 localization to cell peripheries which may be indicative of hemichannel formation that allows for the molecular transport between the cellular cytosol and the ECM. RNAi-treated and untreated cells could be seeded and subjected to the addition of ethidium bromide (EtBr) directly to their growth media. EtBr is a fluorescent dye that enters cells only through functional hemichannels. Once inside, it can translocate into the nucleus, intercalate itself within DNA and fluoresce (Schadzek et al. 2018). Cells containing dye could either be imaged and counted, or they could be subjected to flow cytometry for quantification of entire cell populations. Functional assays to determine how a loss of AmotL1 affects cell-cell communication will certainly provide key insight into the mechanisms promoting carcinogenesis. Should these experiments yield novel results, the clinical implications may offer life-changing benefits to both the patient and scientific communities.

AmotL1 knockdown appears to influence actin dynamics, resulting in a loss of stress fibers and focally-localized actin.

Throughout these experiments, I consistently observe that AmotL1 knockdown causes cells to experience reduced proliferation in culture. I have attempted to quantify this observation using an MTT assay but to no avail. This technique utilizes NADPH-dependent oxidoreductases to reduce tetrazolium MTT dye and serves as a measure of mitochondrial activity. As the number of cells increases, there is increased reduction of MTT detectable by spectrophotometry. Seeding at 20,000 cells per well of a 96-well plate, I found that cells began to clump together and die after two days of growth. In future studies I would suggest seeding at 10,000 cells per well.

In addition to decreased proliferation, knockdown of AmotL1 through RNAi leads to cell flattening. Affected cells appear larger than control cells and are rounder and more pancake-like in their morphology (see Figure 8). To help explain these trends, I investigated changes in the actin cytoskeleton, as this serves to guide both cellular morphology and establish polarity.

Using phalloidin as a red fluorescent dye that stains filamentous F-actin, both control cells and those treated with RNAi against AmotL1 were imaged. Results are shown in Figure 9. Since RNAi is not 100% efficient across all treated cells, AmotL1 was also stained with the intention of visually identifying cells with differential knockdown of the protein. This could allow for the selection of a field of view that contains cells with normal or reduced AmotL1 expression and compare changes in actin organization. I had predicted that as these astrocytes flatten, they would experience greater adhesion to any extracellular surfaces. This could be validated by general increases in the amount of focal adhesions,

which appear as speckles near the cell body, as well as increased stress fiber formation. However, the opposite effect was observed upon imaging. Flattened cells with successful AmotL1 knockdown had notably less focally-localized actin, less stress fibers and an increase in cortical actin.

Previous work conducted by the Wells laboratory has identified similar changes in actin organization depending on LATS1/2 (Large Tumor Suppressor Protein 1/2) kinase activity and the phosphorylation status of Angiomotin-protein-130 (Amot-p130). Cells with low expression of Amot-p130 are characterized by high LATS activity. In MCF7 breast cancer cells, it appears that LATS phosphorylates Amot-p130, causing a shift in the distribution of actin from active stress fibers to the cellular cortices. Likewise, exogenous expression of Amot1p-30 causes an inverse reduction in LATS activity. This event is followed by visual increases in the formation of stress fibers and focally-localized actin attachments to the ECM due to the dephosphorylated status of Amot-p130 (unpublished data). I have essentially repeated these observations in human embryonic astrocytes. With reduced AmotL1 levels and phosphorylation in cells, these conditions promote stress fibers. Furthermore, to identify the effects of differentiation on cytoskeletal arrangements, cells were raised in Barris Neurobasal media. I predicted that differentiation would lead to increases in LATS activity, which is consistent with previous findings in the Wells laboratory. If true, high LATS activity and phosphorylation of AmotL1 would increase the relative concentration of cortical actin. Shown in Figure 8C, similar actin patterns are observed only in the AmotL1-knockdown cells.

As these cells flatten, they lose stress fibers, focally-localized actin and develop a band of cortical actin around their peripheries. Uninfected cells and cells treated with the

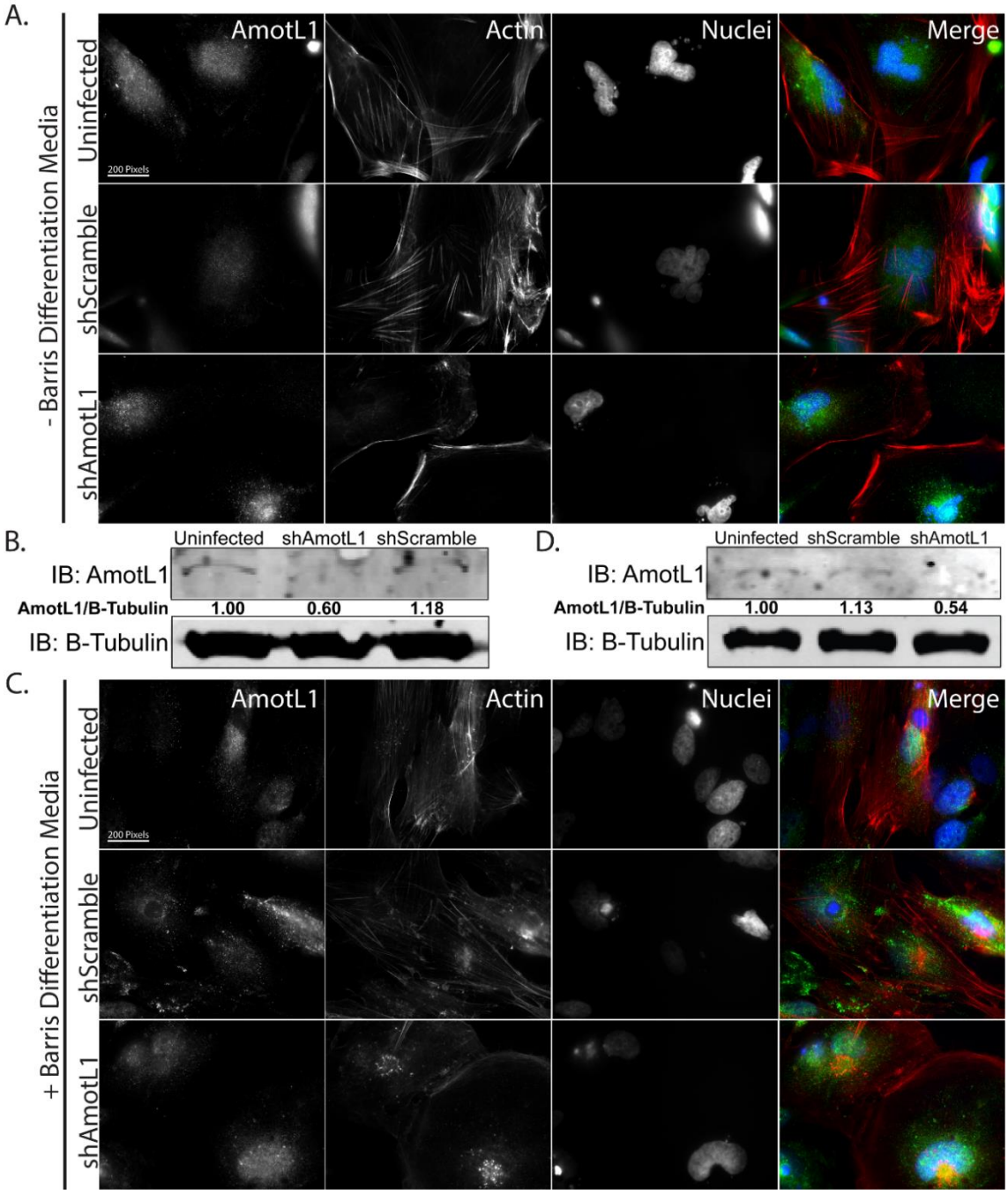

Figure 8: Actin cytoskeletal changes in hEAT cells upon differentiation and treatment**. A.** Cells grown in standard DMEM complete for hEATs. Upon AmotL1 knockdown, cells become significantly rounded and experience losses in both stress fibers and focally-localized actin. Instead these cells experience increases in their distribution of cortical actin. **B.** Western blot analysis for cells shown in A. **C.** Cells grown in Barris Neurobasal media. Even in the presence of pro-differentiation signals, AmotL1 knockdown causes a reduction in the formation of stress fibers. **D.** Western blot analysis for cells shown in C.

shScramble lentiviral RNAi continue to exhibit stress fibers, indicating that AmotL1 may be playing an even more critical role in regulating actin dynamics than has been previously considered. Other conditions were investigated, in which combinations of ZO-1 and actin, well-established binding partners, and AmotL1 and ZO-1 were stained to see if there is any form of colocalization that may be indicative of a binding interaction. Like previous findings, I repeatedly observe increased distribution of ZO-1 to cell peripheries and contacts upon AmotL1 knockdown, as well as upon differentiation using Barris Neurobasal media (See Figures 11-12, in Appendix A).

To explain these phenomena, I hypothesize that AmotL1 may be influencing the activity of RhoA GTPase which stimulates the formation of filamentous actin (e.g. stress fibers). Unphosphorylated AmotL1 may indirectly activate RhoA through the stimulation of Syx protein. Syx, also named TECH or PLEKHG5, is a RhoA-specific synectin-binding guanine exchange factor that is localized to cellular membranes through its interaction with the Crumbs polarity complex. Upon binding, Syx activates RhoA through an exchange of GTP for its bound GDP (Dachsel et al. 2013). Upon binding to GTP, RhoA undergoes a conformation change to become active (Truebestein et al. 2015). It may then interact with ROCK1 (Rho-associated, coiled-coil-containing kinase) or Cdc42 (Cell division control protein 42 homolog) to induce downstream activation of actin nucleators (Azab et al. 2009, Watson et al. 2011, Maekawa 2009, Maekawa 1999, Tapon et al. 1997). These nucleators include mDiA1/2 which allow for the formation of new stress fibers throughout the cytoskeleton, and the Arp2/3 (actin-related protein 2/3) complex which is activated upon binding by WASP (Wiskott–Aldrich syndrome protein) members, respectively (Padrick et

al. 2011). Active Arp2/3 may then bind the sides of filamentous F-actin and stimulate nucleation of branched actin fiber formation.

To investigate these principles, I utilized lentiviruses to induce expression of exogenous AmotL1 WT, AmotL1 S262D, or AmotL1 262A mutants in both hEAT and A172 human glioblastoma cell lines. The WT was used as a control and mutants were utilized to investigate the role of AmotL1 phosphorylation status on stress fiber formation. Both constructs were designed by the Wells laboratory prior to my entry. The S262D mutant has been designed to mimic a phosphorylated state. I predicted that cells expressing this mutant would be less able to activate RhoA, thus cells would have reduced amounts of stress fibers. Under these conditions, I anticipated that this would lead to the development of a cortical actin band as seen in the AmotL1-knockdown cells of Figure 8. Likewise, the S262A mutant was designed to prevent phosphorylation of AmotL1, thus promoting its activation of RhoA via Syx and allowing for the formation of new stress fibers.

As an additional factor I did or did not overexpress Nedd4-1, a HECT-domain-containing member of the AIP4 E3 ubiquitin ligase family. Previous studies have suggested that phosphorylated AmotL1, similar to angiomotins, can activate Nedd4-1 (Wang et al. 2012). Active members of the AIP4 family, such as Smurf1, can ubiquitinate and lead to the degradation of both RhoA and AmotL1 as a form of negative feedback (Wang et al. 2006, Bryan et al. 2005). Thus, I predicted that cells expressing the AmotL1 S262D mutant *and* Nedd4-1 would lead to increased degradation of RhoA, resulting in a loss of stress fibers because of its inability to activate mDIA1/2, WASP/WAVE and Arp2/3 complexes needed for actin nucleation.

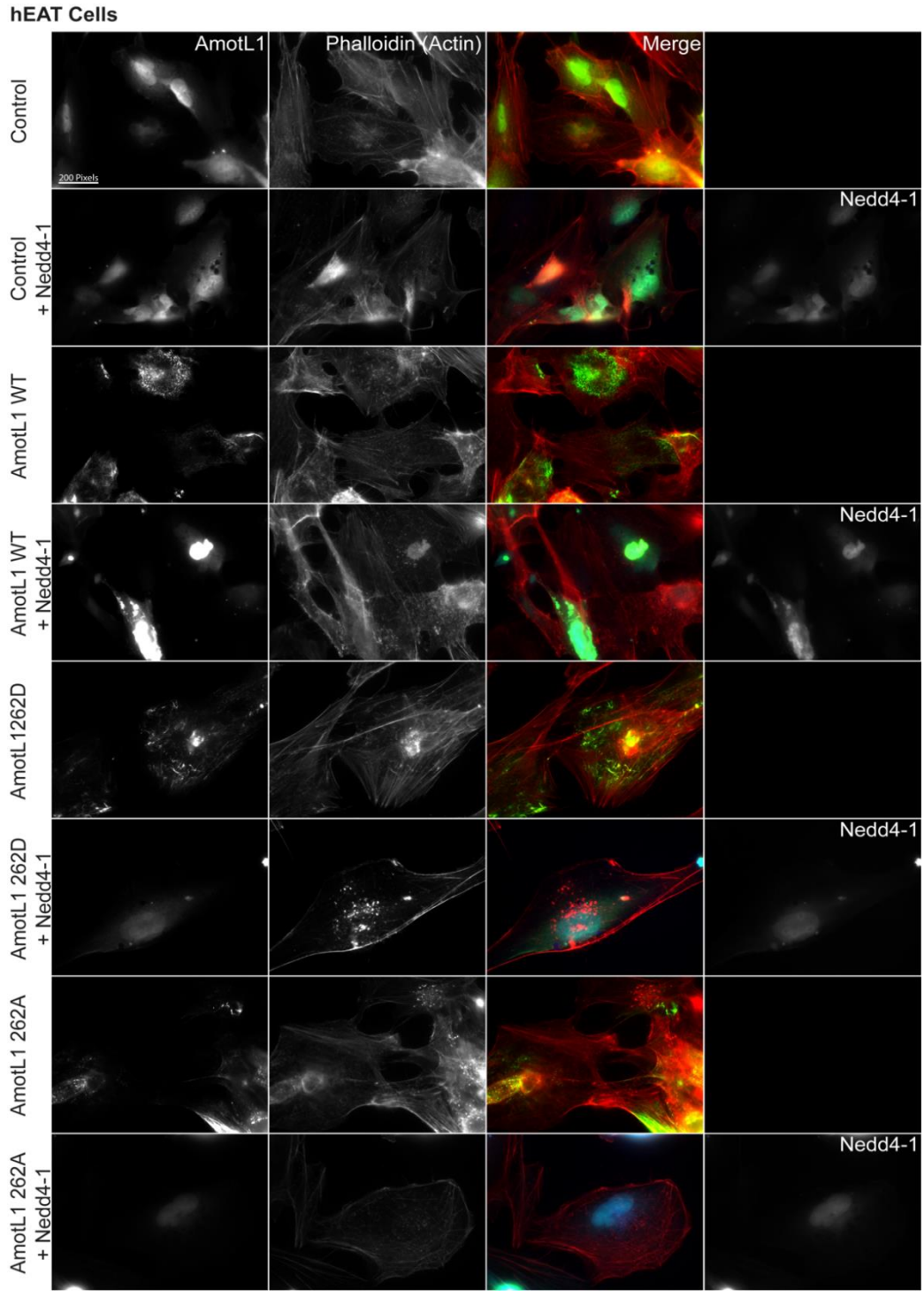

Figure 9: Effects of AmotL1 phosphorylation status and possible ubiquitination on actin organization in hEAT cells**.** An AmotL1 262D mutant, upon Nedd4-1 expression, results in reduced stress fiber formation. Upon expression of Nedd4-1, there is a colocalization of Nedd4-1 and AmotL1 within the nucleus.

In hEAT cells, many of these predictions were validated by my results (See Figure 9). Cells treated with a control empty vector and AmotL1 WT conditions, with or without the addition of Nedd4-1, present abundant stress fibers and focal adhesions throughout the cell body. When cells express the AmotL1 S262D mutant, they continue to exhibit stress fiber formation despite their irreversible phosphorylation status. Upon the expression of Nedd4-1, however, there is a significant change in the cytoskeletal actin arrangement of these mutant cells. There is reduced stress fiber formation and the presence of focal adhesion-like speckles near the cell body. These observations suggest that AmotL1 phosphorylation can influence actin cytoskeletal arrangements in a Nedd4-1-dependent manner. It may be that Nedd4-1 requires the activation from phosphorylated AmotL1 to ubiquitinate and degrade RhoA via the 26S proteasome; however, the interactions and molecular mechanism warrant further investigation to elucidate the definitive roles of each protein. Cells expressing the AmotL1 S262A mutant, which prevents AmotL1 phosphorylation and Nedd4-1 activity, remain abundant with stress fibers and the production of exogenous Nedd4-1 appears to have no impact on actin. This is likely due to the Nedd4-1 dysfunction brought about by the AmotL1 mutation.

Upon expression of Nedd4-1 in both hEAT and A172 cells (Figures 9 and 10), AmotL1 and Nedd4-1 to consistently colocalize punctate regions within the cell body that appear to be nuclear. This is highly interesting, as there is limited evidence proposing the translocation of AmotL1 into the nucleus although it can promote the transcription of certain genes. Taken together, this observation suggests that this may be a novel finding. Related angiomotins have been shown to exist in the nucleus and studies suggest that translocation may require sumoylation and binding to importins (Zhu et al. 2017).

However, AmotL1 has an arginine residue within its nuclear localization sequence preventing sumoylation. This suggests that a different post-translational modification is required for import, such as ubiquitination.

Of course, I am limited in making these claims. I did not include a nuclear dye within the immunofluorescent procedure for these experiments due to my choices in fluorescently-labeled proteins and phalloidin stain. I intend on repeating this experiment using the YFP-labelled AmotL1 variations, the CFP-labelled Nedd4-1 and propidium iodide for nuclear staining in order to validate the localization of AmotL1 to the nucleus. Since translocation occurs only in the presence of Nedd4-1, it seems that ubiquitination of AmotL1 by this E3 ligase is essential. In the future, it would be interesting to generate cells that express an AmotL1 K488R mutant that prevents its ubiquitination. I predict that this site-directed mutagenesis will prevent Nedd4-1 from acting on AmotL1, thus preventing its translocation into the nucleus.

Future studies should investigate expression of RhoA, and other proteins proposed by my model, upon changing experimental conditions. Cells could be infected to express AmotL1 S262D alone, Nedd4-1 alone or combined and Western blot analysis used to quantify RhoA protein levels. I expect RhoA to have higher expression in both single treatments; however, upon combination, I anticipate that the phosphorylated AmotL1 would activate Nedd4-1, leading to the ubiquitination and proteasomal degradation of RhoA, resulting in less protein on the immunoblot. These data, if true, would further validate the observation of decreased stress fiber formation seen in AmotL1- knockdown cells. Should these results indicate that RhoA protein is affected, it may prove beneficial to explore its degradation. Cells could be treated with cycloheximide to block new RhoA

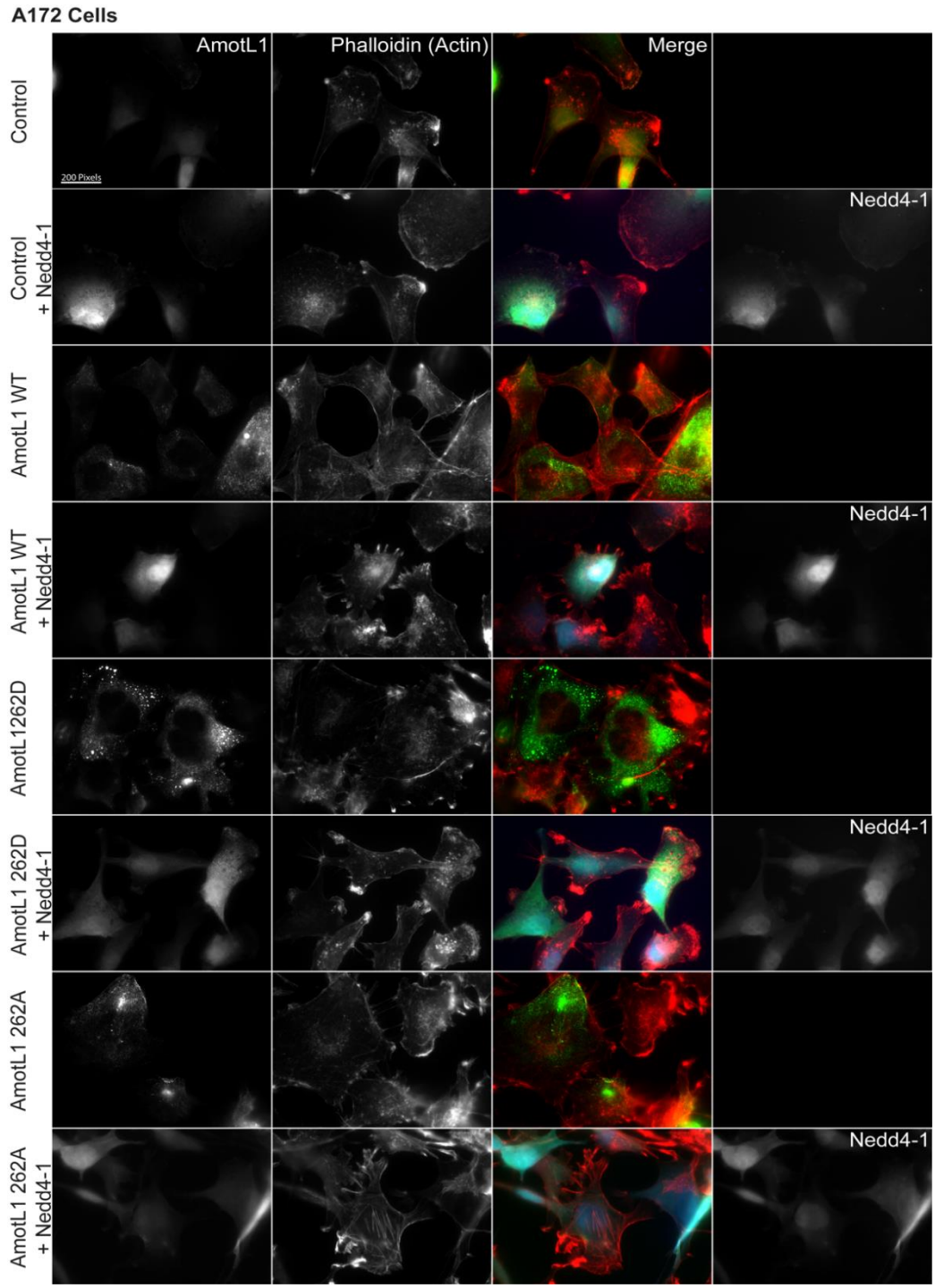

Figure 10: Effects of AmotL1 phosphorylation status and possible ubiquitination on actin organization in A172 cells**.** GBM cells differ in actin organization compared to control hEAT cells. Upon expression of Nedd4-1, there is a colocalization of Nedd4-1 and AmotL1 within the nucleus. It appears that the AmotL1 262D mutant as well as the AmotL1 wildtype upon expression of NEDD4-1 stimulates formation of filipodia.

translation, then the degradation of remaining pre-existent RhoA could be tracked overtime amongst the different treatment groups. I would also like to better understand the mechanism by which RhoA is targeted for proteasomal degradation (Wei et al. 2013, Wang et al. 2006, Bryan et al. 2005). Using K7, K48, and K63 ubiquitin mutants, the amino acid residues and branching patterns required for the degradation of RhoA could be identified (Ohtake et al. 2018).

These experiments have allowed me to define the effects of expressing AmotL1 or its mutants that mimic various phosphorylation statuses at serine 262 by the LATS1/2 kinases. This has allowed for the validation of previous findings made by the Wells laboratory. By combining these conditions with exogenous expression of the NEDD4-1 E3 ubiquitin ligase, my data suggest that ubiquitination of AmotL1 may be more important that previously considered. This post-translational modification is responsible for both the regulation of AmotL1 phosphorylation status and the potential translocation of AmotL1 into the nucleus. Expression of an AmotL1 S262D mutant in combination with NEDD4-1 results in a profound loss of actin stress fibers, likely due to the degradation of filamentous actin-promoting proteins which I currently believe is RhoA. Taken together, these data create a story in which AmotL1 is a central player in guiding cell behavior. In addition to its known roles in preventing oncogenic expression via regulation of YAP/TAZ, I have shown that AmotL1 expression and phosphorylation status act to dictate cell morphology by regulating the dynamics of the actin cytoskeleton. Changes in polarity and architecture may have consequences that have not yet been thoroughly investigated, especially in the context of GBM. These properties make AmotL1 a novel therapeutic target in understanding the mechanisms of carcinogenesis and in the global combat against cancer.

Appendices

Appendix A

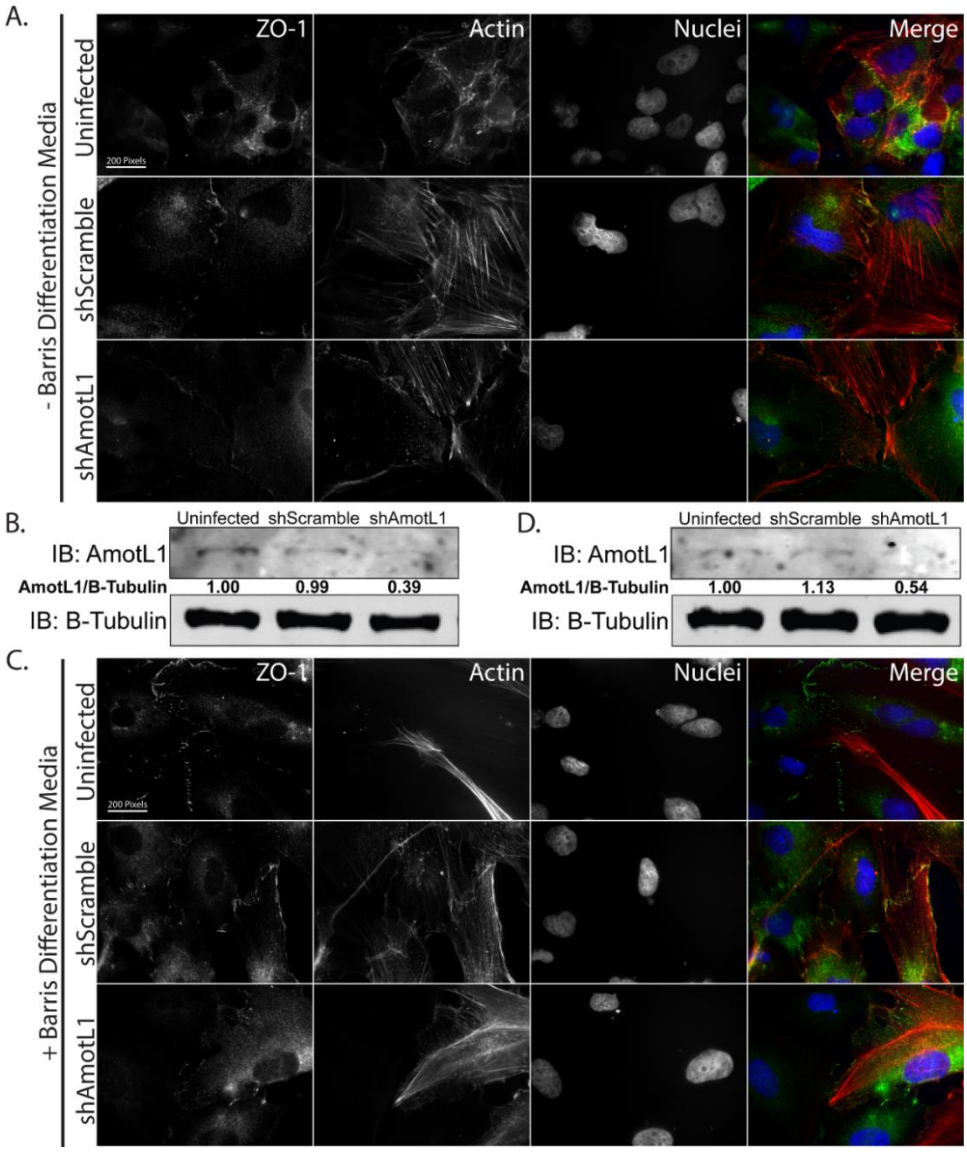

Figure A-11: Changes in actin cytoskeletal arrangements and colocalization with ZO-1 in hEAT cells upon differentiation and treatment. **A.** Cells grown in standard DMEM complete for hEATs. Upon knockdown of AmotL1, cells become rounded, lose stress fibers and focally-localized actin yet experience increased distribution of cortical actin. In the shAmotL1 images, it appears that 2/3 cells have AmotL1 knockdown; the third continues to demonstrate stress fiber formation. **B.** Western blot analysis for cells shown in A. **C.** Despite growth in Neurobasal media, cells with AmotL1 knockdown have reduced stress fiber formation. **D.** Western blot analysis for cells shown in C.

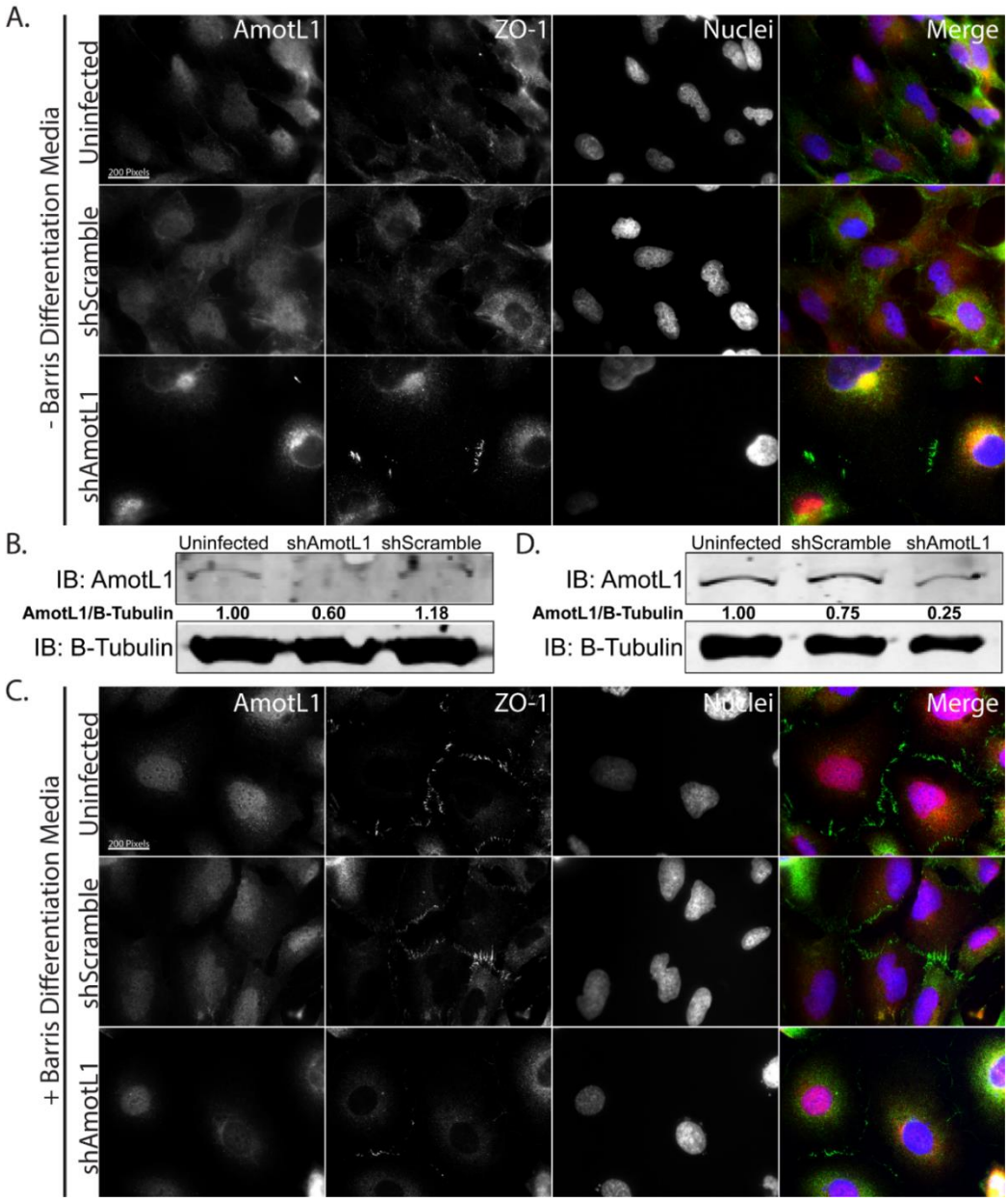

Figure A-12: AmotL1 and ZO-1 colocalization in hEAT cells upon differentiation and treatment**. A.** Cells grown in standard DMEM complete for hEATs. Upon AmotL1 knockdown, cells become rounded and experience increased cortical localization of ZO-1. This is indicative of increased gap junction formation. **B.** Western blot analysis for cells shown in A indicates 40% knockdown of AmotL1. **C.** Cells grown in Barris Neurobasal meida. Differentiation increases the relative abundance of ZO-1 to cell-cell contacts, presumably at gap junctions. **D.** Western blot analysis for cells shown in C shows successful AmotL1 knockdown by RNAi.

A.

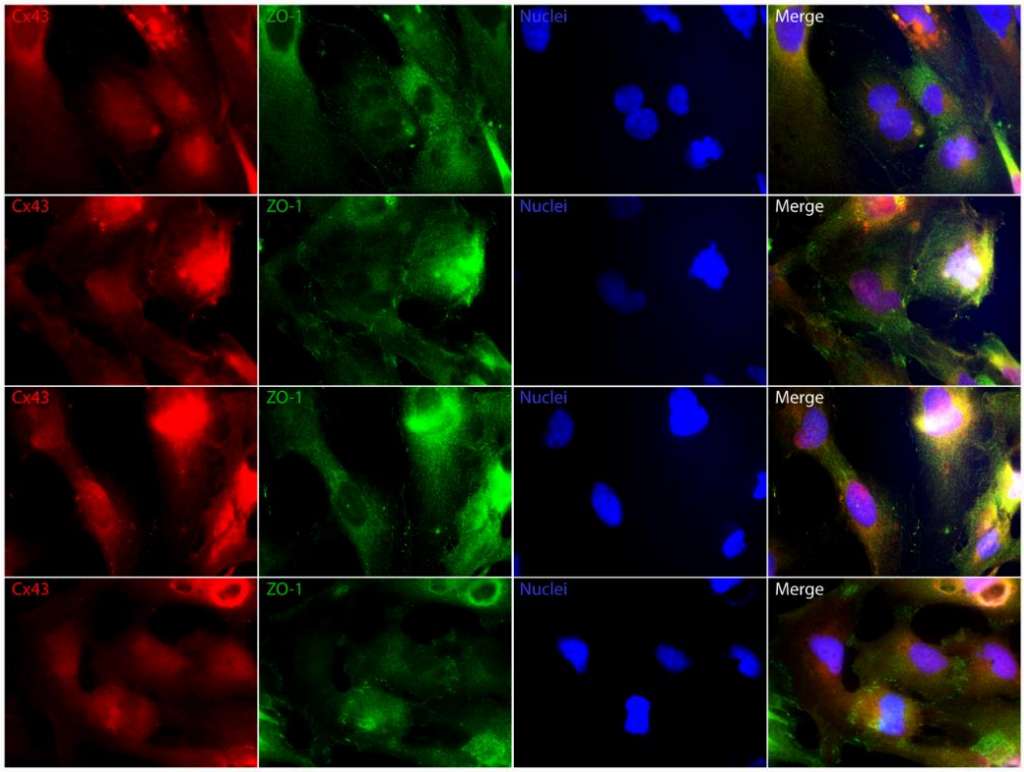

B.

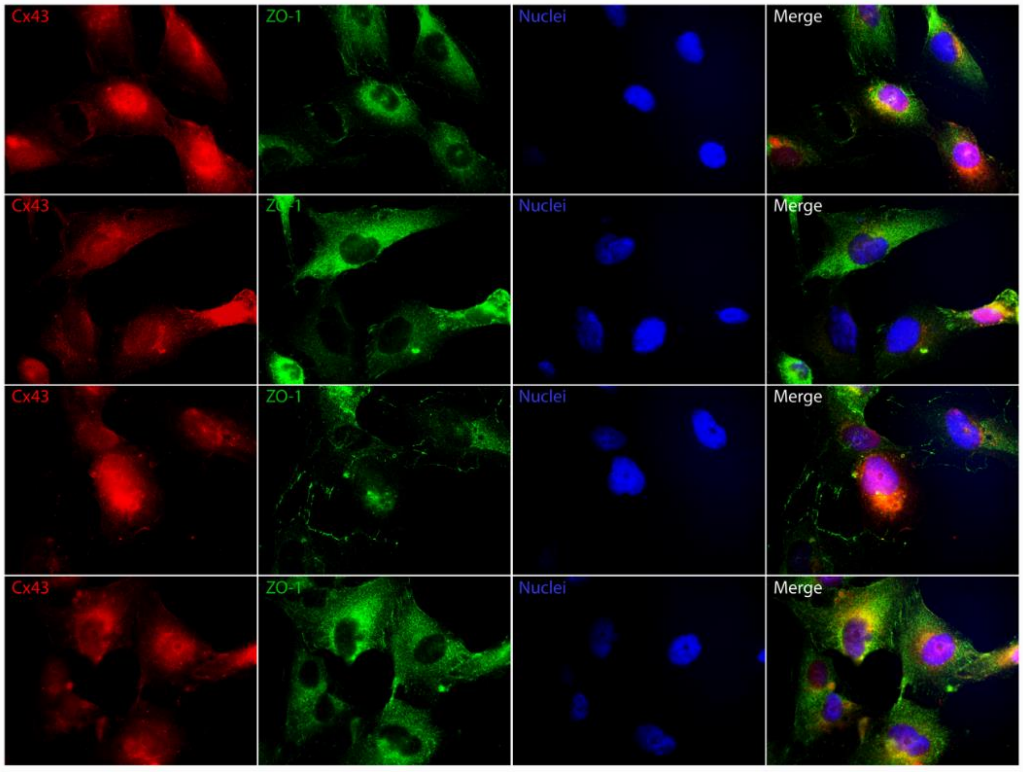

Figure A-13: Cx43 and ZO-1 colocalization in uninfected cells**. A.** Colocalization in control hEAT cells.

B. Colocalization in hEAT Cx43 Untagged cells.

A.

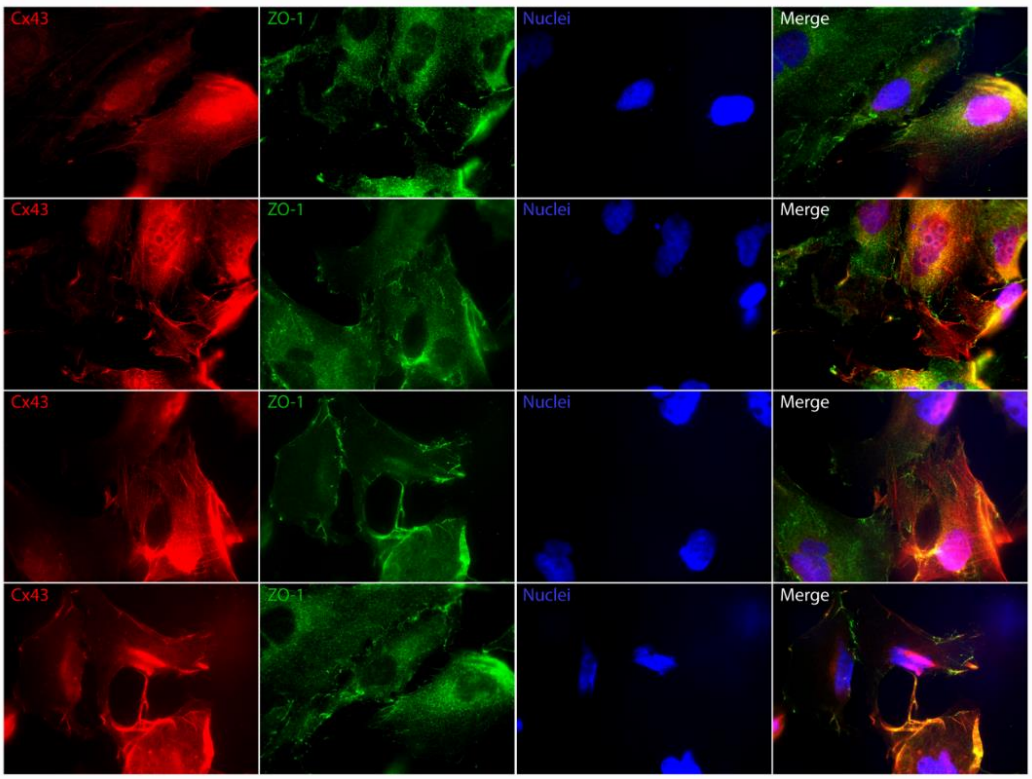

B.

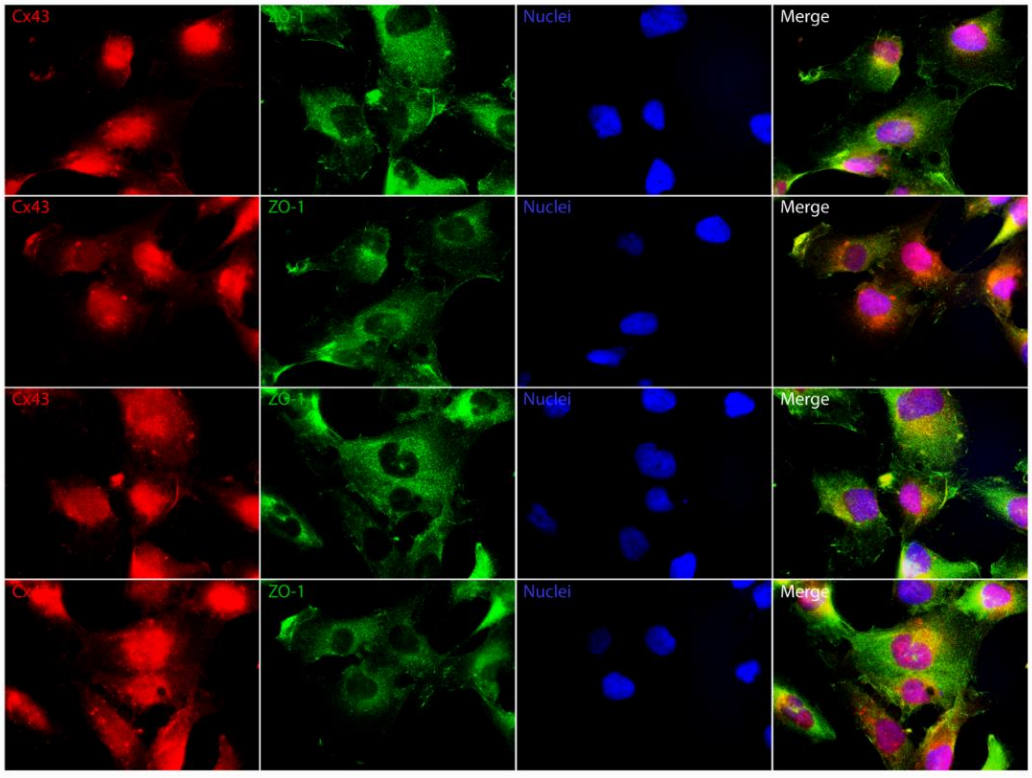

Figure A-14: Cx43 and ZO-1 colocalization in shScramble-treated cells. **A.** Colocalization in control hEAT cells. **B.** Colocalization in hEAT Cx43 Untagged cells.

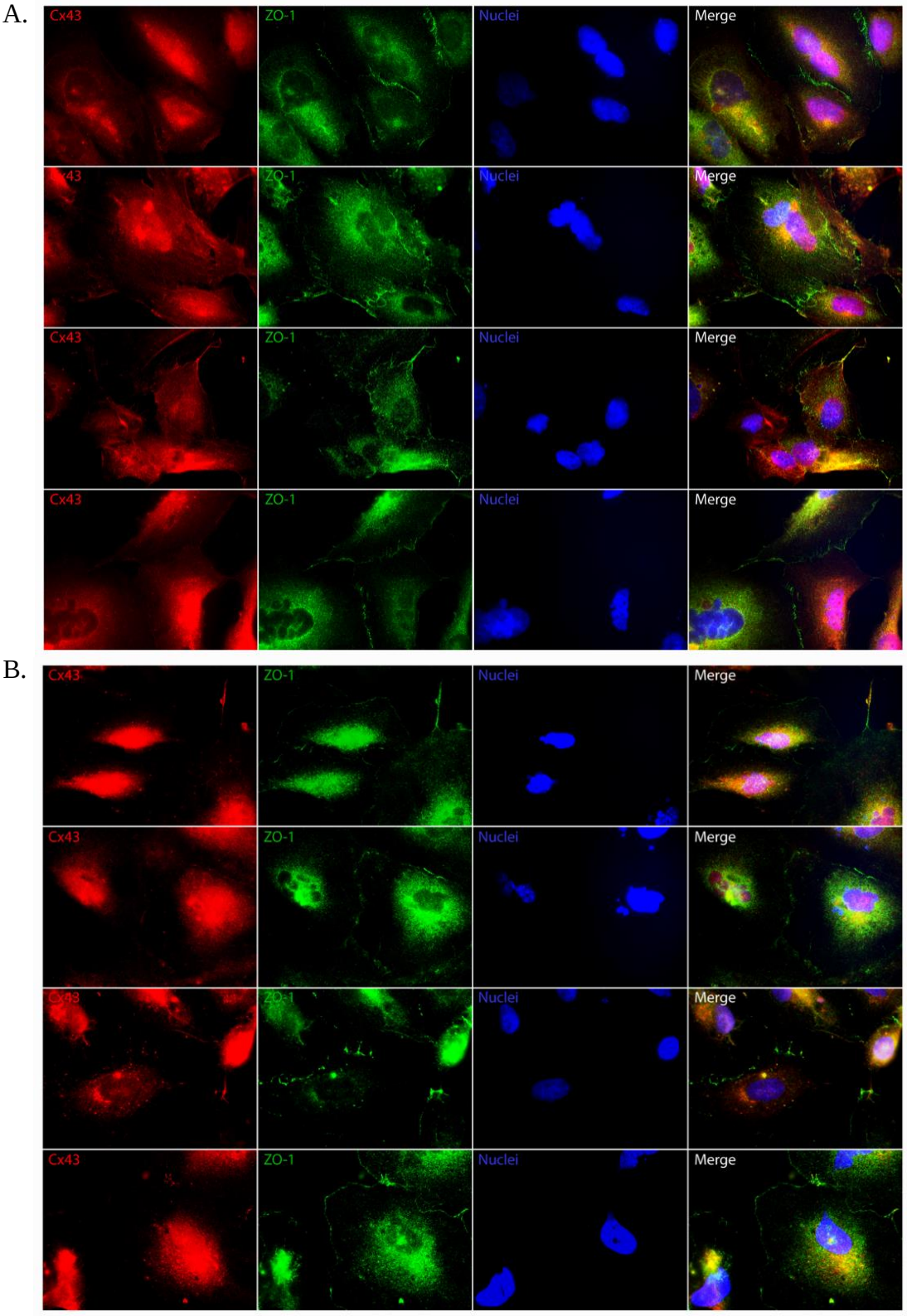

Figure A-15: Cx43 and ZO-1 colocalization in shAmotL1-treated cells**. A.** Colocalization in control hEAT cells. **B.** Colocalization in hEAT Cx43 Untagged cells.

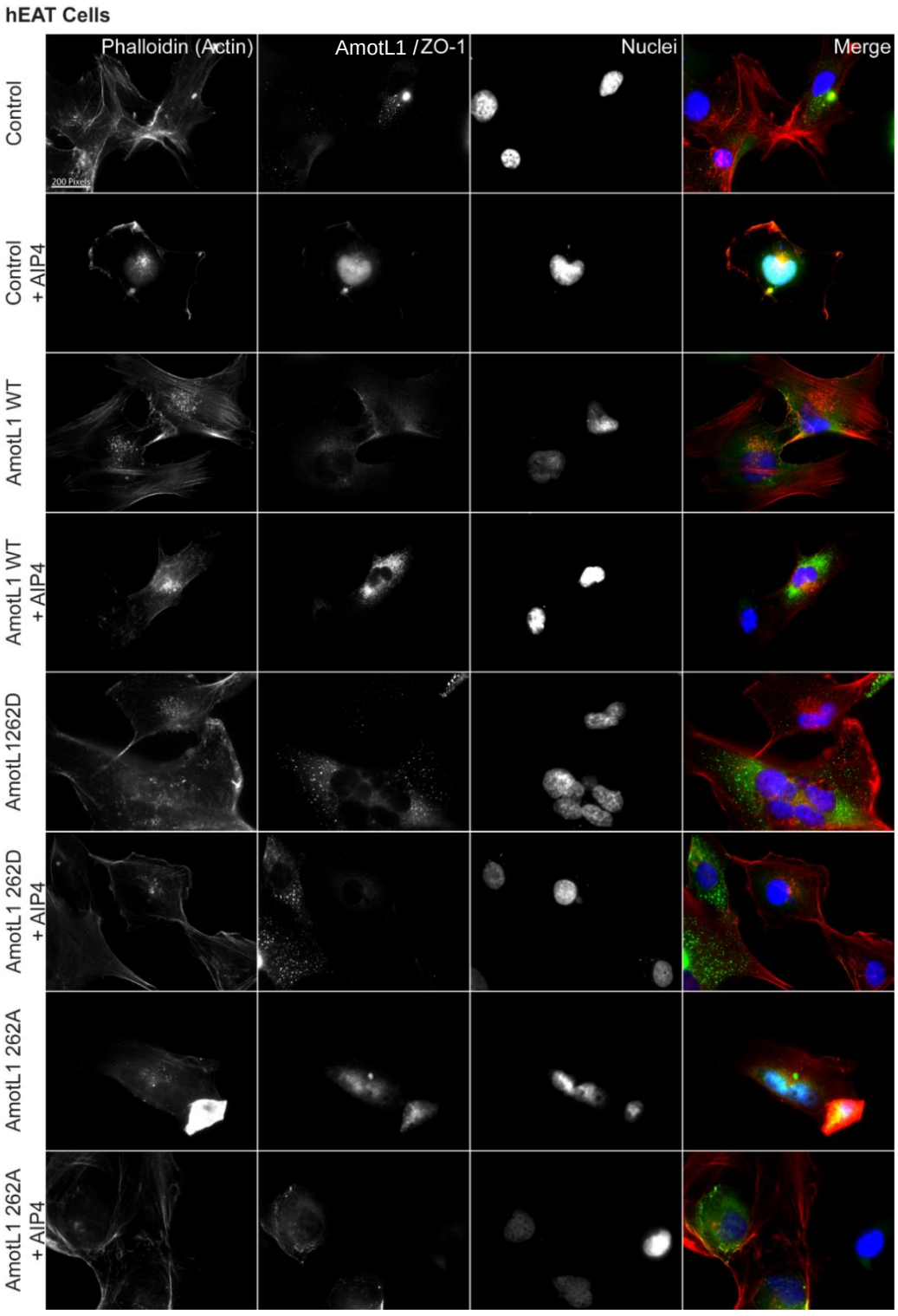

Figure A-16: Preliminary exploration of the effects of AmotL1 phosphorylation status and ubiquitination on actin cytoskeletal organization in hEAT cells**.** ZO-1 was stained with a monoclonal ZO-1 antibody with emission at 488 nm which conflicted with YFP-AmotL1.

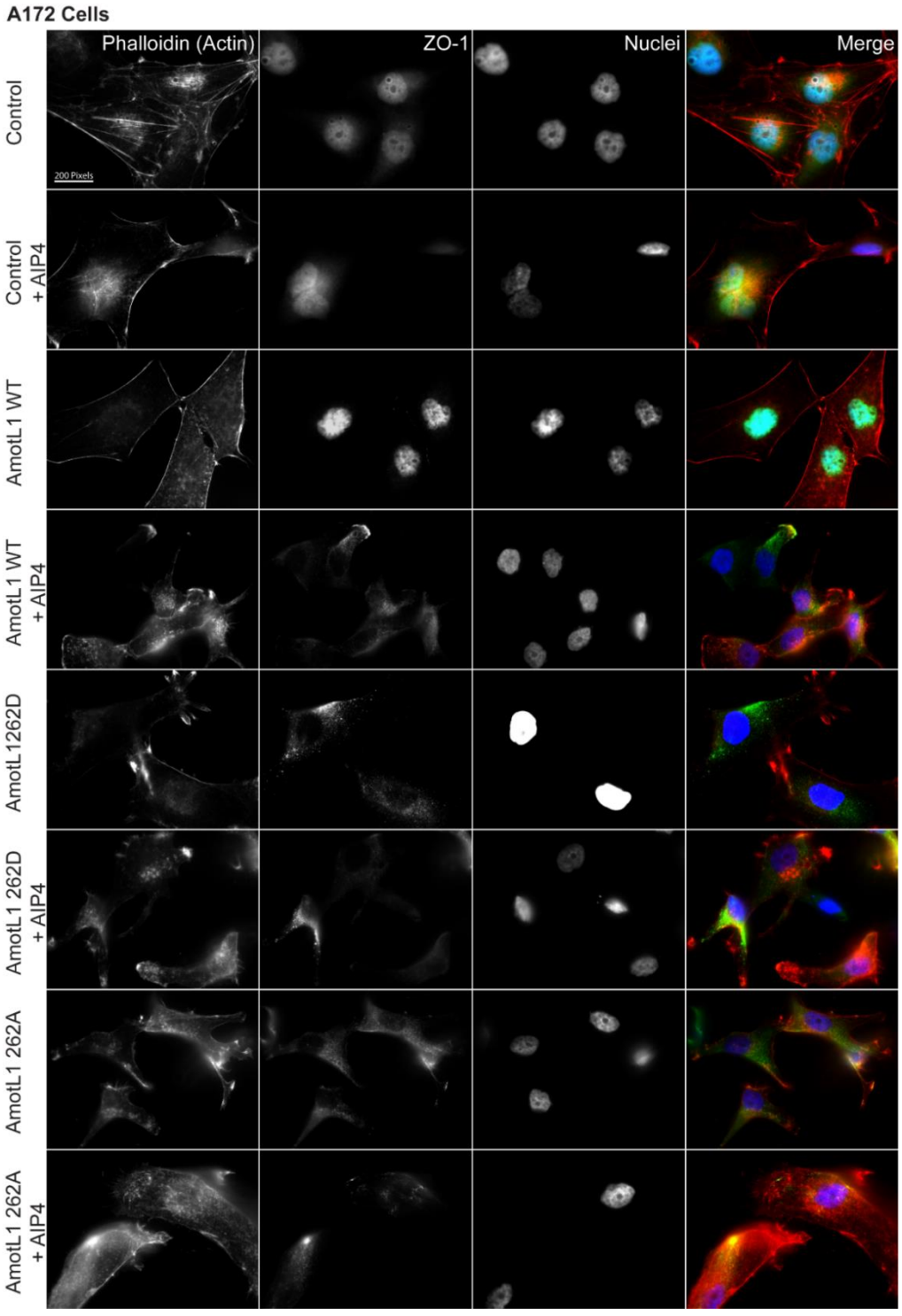

Figure A-17: Preliminary exploration of the effects of AmotL1 phosphorylation status and ubiquitination on actin cytoskeletal organization in A172 cells**.** ZO-1 was stained with a monoclonal ZO-1 antibody with emission at 488 nm which conflicted with YFP-AmotL1. AmotL1 262D mutants have extensive filopodia.

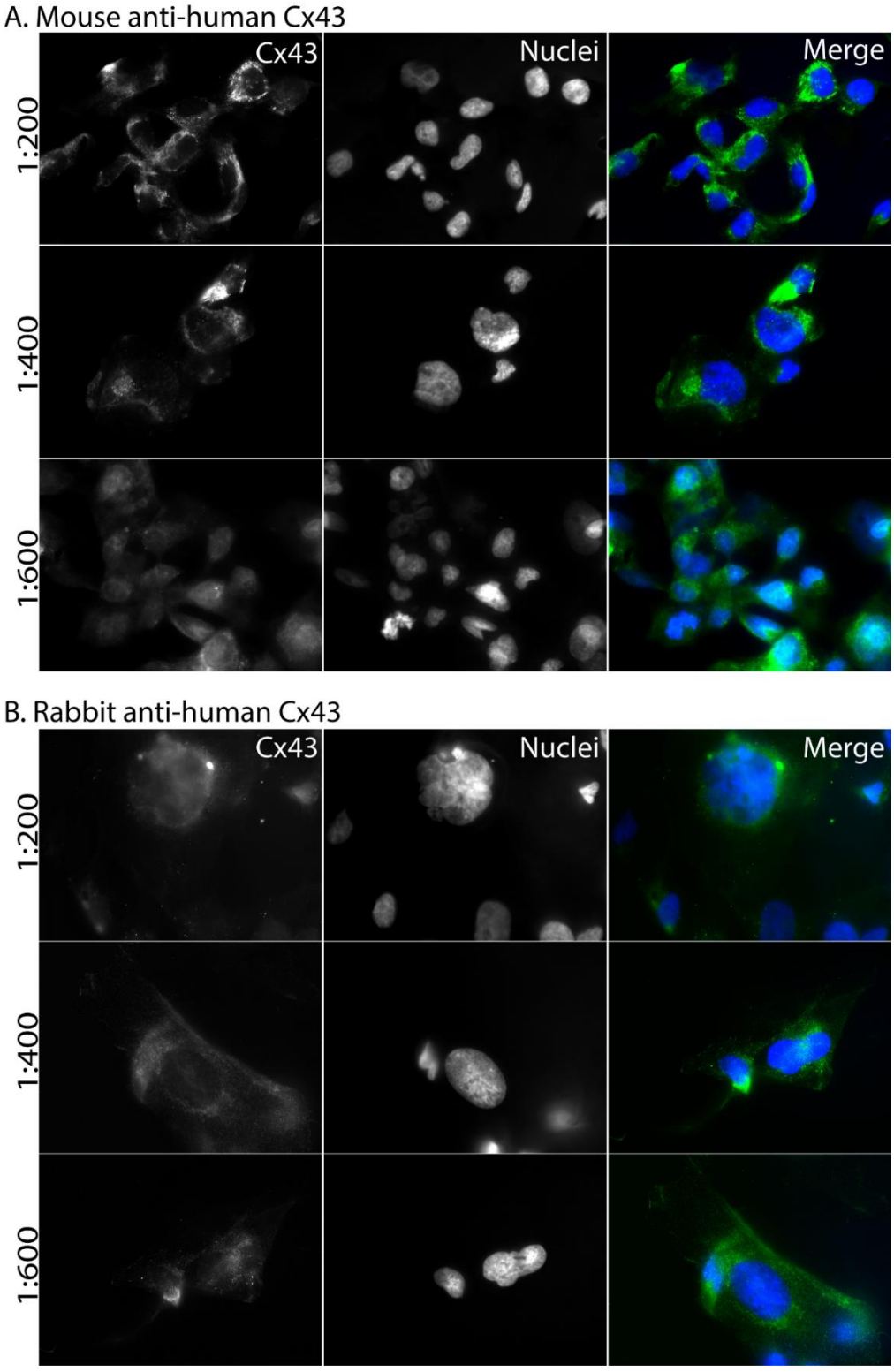

Figure B-18: Optimization of Cx43 antibodies.

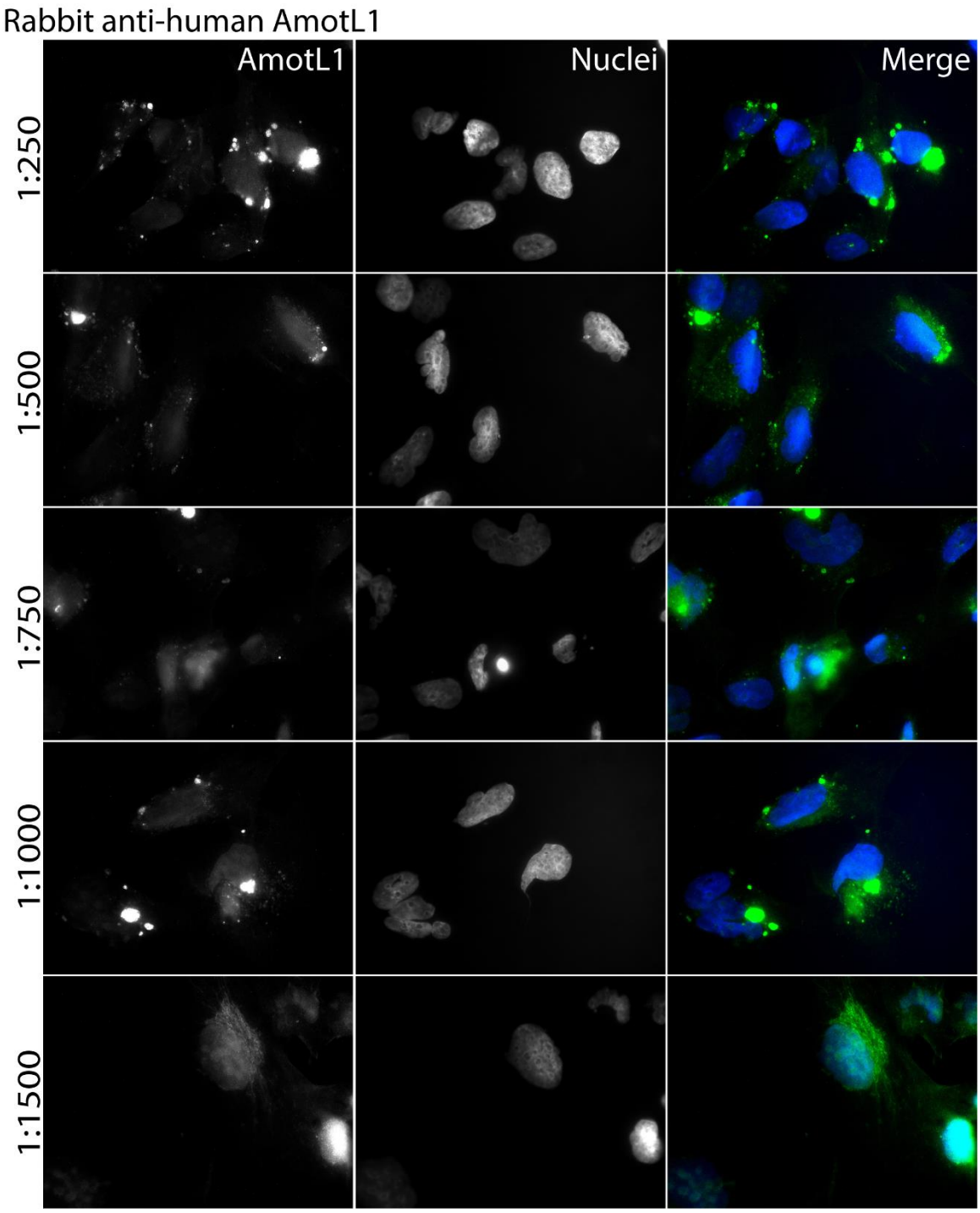

Figure B-19: Optimization of AmotL1 antibody**.** Made in house by the Wells laboratory.

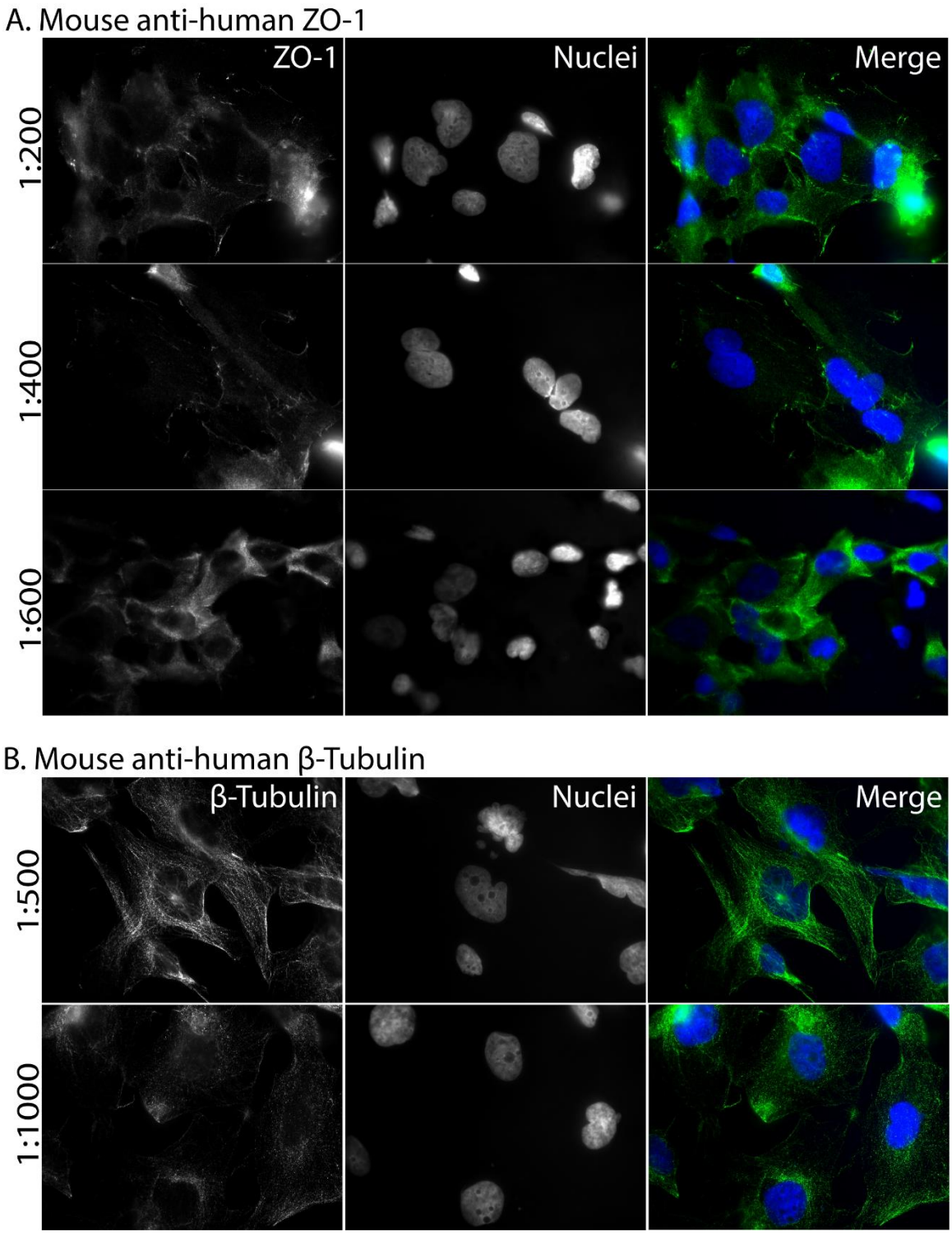

Figure B-20: Optimization of ZO-1 and β-Tubulin antibodies**. A.** Attempted ZO-1 antibody dilutions. **B.** Attempted β-Tubulin antibody dilutions.

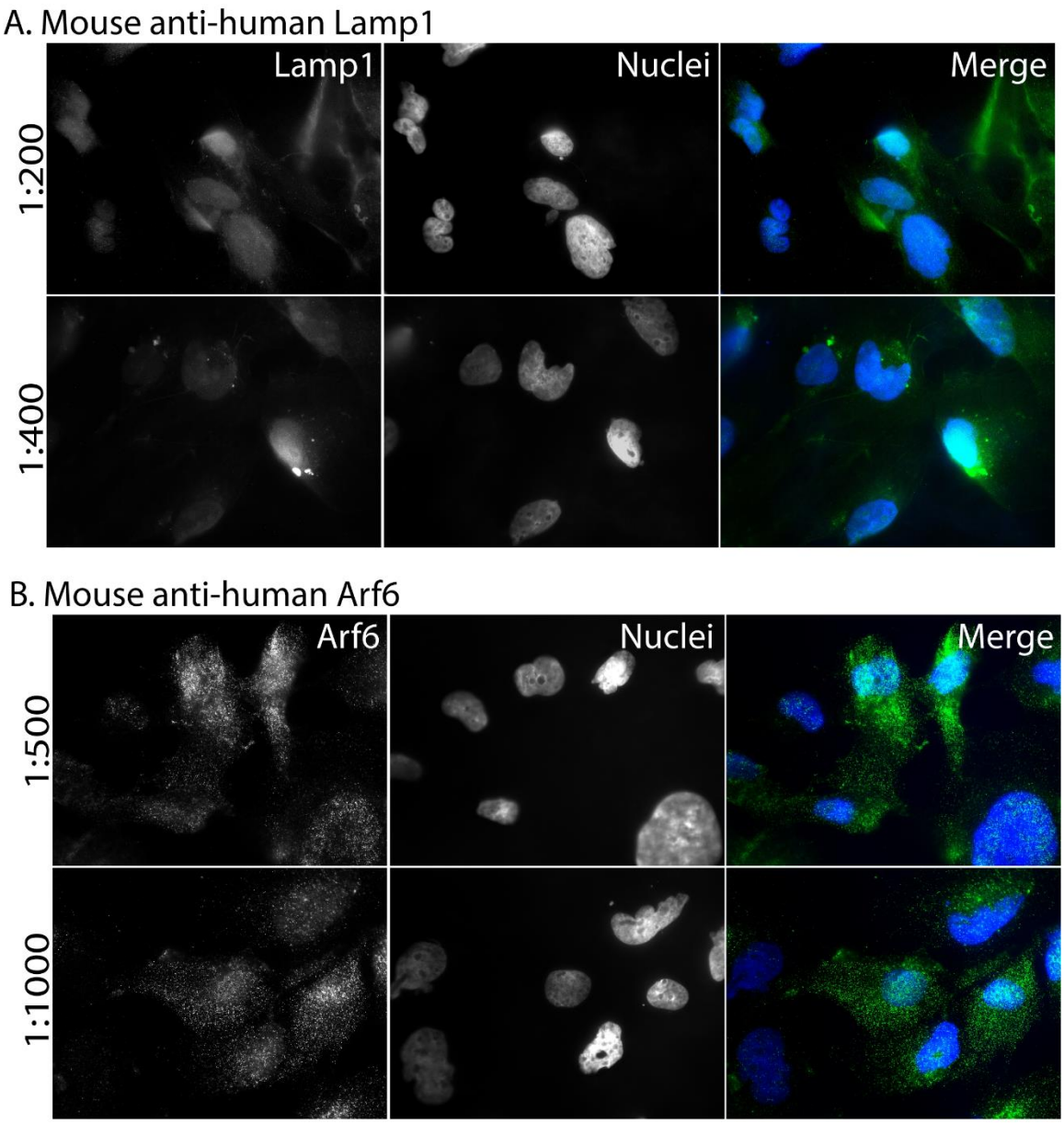

Figure B-21: Optimization of Lamp1 and Arf6 antibodies**. A.** Attempted Lamp1 antibody dilutions. **B.** Attempted Arf6 antibody dilutions.

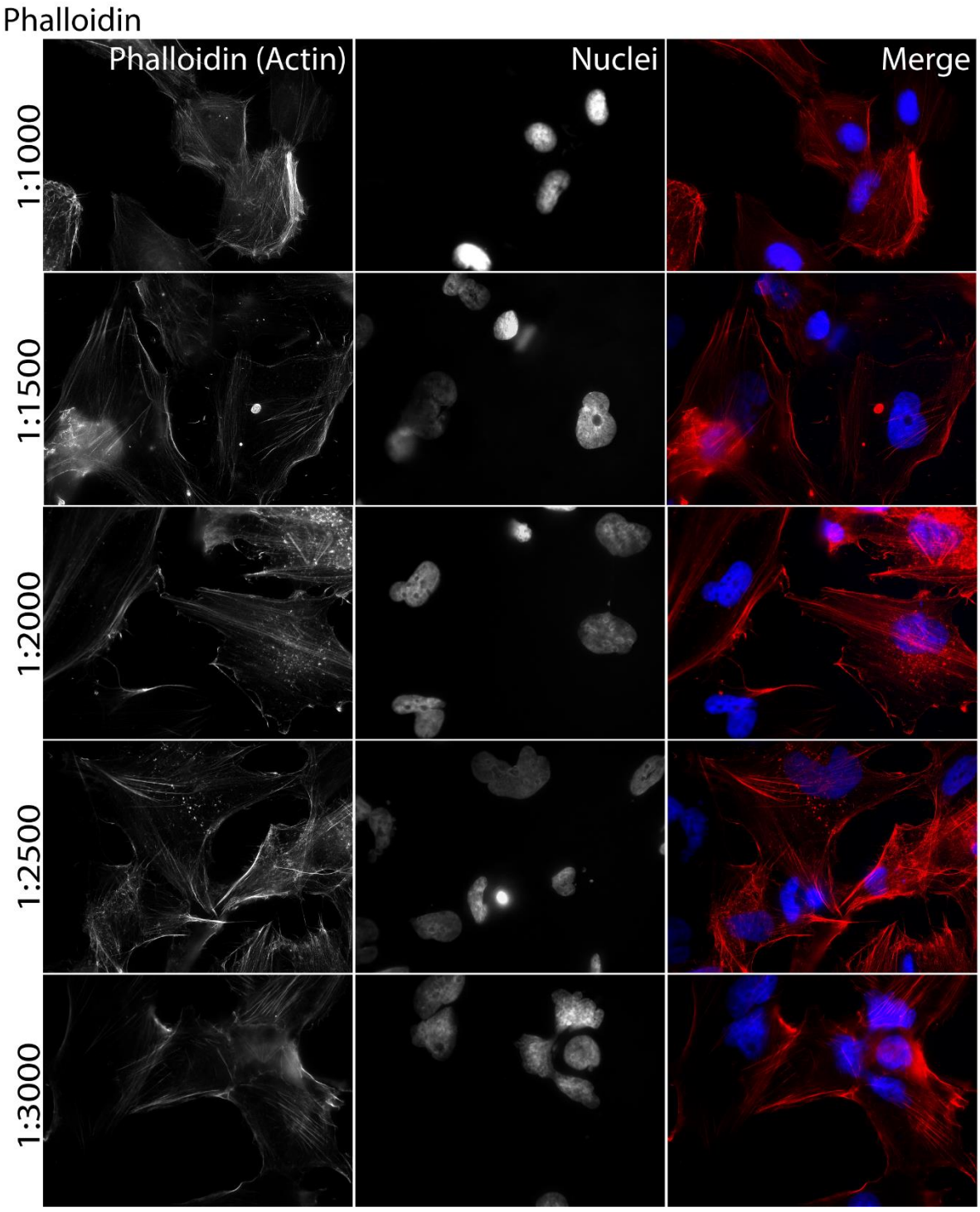

Figure B-22: Optimization of phalloidin**.**

References

Ambesajir, Anghesom, et al. “RNA Interference: A Futuristic Tool and Its Therapeutic Applications.” *Saudi Journal of Biological Sciences*, vol. 19, no. 4, Oct. 2012, pp. 395–403., doi:10.1016/j.sjbs.2012.08.001.

Amankulor, Nduka M., et al. “Mutant IDH1 Regulates the Tumor-Associated Immune System in Gliomas.” *Genes & Development*, vol. 31, no. 8, 12 Apr. 2017, pp. 774–786., doi:10.1101/gad.294991.116.

Azab, A. K., et al. “RhoA and Rac1 GTPases Play Major and Differential Roles in Stromal Cell-Derived Factor-1-Induced Cell Adhesion and Chemotaxis in Multiple Myeloma.” *Blood*, vol. 114, no. 3, 14 May 2009, pp. 619–629., doi:10.1182/blood-2009-01-199281.

Baas, Annette F, et al. “LKB1 Tumor Suppressor Protein: PARtaker in Cell Polarity.” *Trends in Cell Biology*, vol. 14, no. 6, June 2004, pp. 312–319., doi:10.1016/j.tcb.2004.04.001.

Baas, Annette F., et al. “Complete Polarization of Single Intestinal Epithelial Cells upon Activation of LKB1 by STRAD.” *Cell Press*, vol. 116, 6 Feb. 2004, pp. 457–466., doi:10.1016/S0092-8674(04)00114-X.

Babica, Pavel, et al. “Scrape Loading/Dye Transfer Assay.” *Methods in Molecular Biology Gap Junction Protocols*, vol. 1437, 21 May 2016, pp. 133–144., doi:10.1007/978-1-4939-3664-9_9.

Berman, Joan W., et al. “HIV-Tat Alters Connexin43 Expression and Trafficking in Human Astrocytes: Role in NeuroAIDS.” *Journal of Neuroinflammation*, vol. 13, no. 1, ser. 54, 2 Mar. 2016, pp. 1–11. *54*, doi:10.1186/s12974-016-0510-1.

Bryan, Brad, et al. “Ubiquitination of RhoA by Smurf1 Promotes Neurite Outgrowth.” *FEBS Letters*, vol. 579, no. 5, 14 Feb. 2005, pp. 1015–1019., doi:10.1016/j.febslet.2004.12.074.

Bukauskas, F. F., et al. “Clustering of Connexin 43-Enhanced Green Fluorescent Protein Gap Junction Channels and Functional Coupling in Living Cells.” *Proceedings of the National Academy of Sciences*, vol. 97, no. 6, 14 Mar. 2000, pp. 2556–2561., doi:10.1073/pnas.050588497.

Campbell, Kirsteen J., and Stephen W. G. Tait. “Targeting BCL-2 Regulated Apoptosis in Cancer.” *Open Biology*, vol. 8, no. 5, May 2018, pp. 180002–1800013., doi:10.1098/rsob.180002.

Chan, Siew Wee, et al. “Hippo Pathway-Independent Restriction of TAZ and YAP by Angiomotin.” *Journal of Biological Chemistry*, vol. 286, no. 9, 4 Mar. 2011, pp. 7018–7026., doi:10.1074/jbc.c110.212621.

Coussens, Lisa M., and Zena Werb. “Inflammation and Cancer.” *Nature*, vol. 420, no. 6917, 19 Dec. 2002, pp. 860-867., doi:10.1038/nature01322

Dachsel, J. C., et al. “The Rho Guanine Nucleotide Exchange Factor Syx Regulates the Balance of Dia and ROCK Activities To Promote Polarized-Cancer-Cell Migration.” *Molecular and Cellular Biology*, vol. 33, no. 24, 14 Dec. 2013, pp. 4909–4918., doi:10.1128/mcb.00565-13.

Davis, Mary. “Glioblastoma: Overview of Disease and Treatment.” *Clinical Journal of Oncology Nursing*, vol. 20, no. 5, 1 Oct. 2016, pp. S2–S8., doi:10.1188/16.cjon.s1.2-8.

Debarba, Lucas Kniess, et al. “The Role of TCPTP on Leptin Effects on Astrocyte Morphology.” *Molecular and Cellular Endocrinology*, vol. 482, 15 Dec. 2019, pp. 62–69., doi:10.1016/j.mce.2018.12.010.

Dhara, Sujoy K., and Steven L. Stice. “Neural Differentiation of Human Embryonic Stem Cells.” *Journal of Cellular Biochemistry*, vol. 105, no. 3, 15 Oct. 2008, pp. 633–640., doi:10.1002/jcb.21891.

Dianati, Elham, et al. “Connexins, E-Cadherin, Claudin-7 and β-Catenin Transiently Form Junctional Nexuses during the Post-Natal Mammary Gland Development.” *Developmental Biology*, vol. 416, no. 1, 1 Aug. 2016, pp. 52–68., doi:10.1016/j.ydbio.2016.06.011.

Faivre, Geraldine, et al. “Clinical Reasoning: Worsening Neurologic Symptoms in a Brain Tumor Patient.” *Neurology*, vol. 85, no. 7, 18 Aug. 2015, pp. e57–e61., doi:10.1212/wnl.0000000000001848.

Fasciani, Ilaria, et al. “Directional Coupling of Oligodendrocyte Connexin-47 and Astrocyte Connexin-43 Gap Junctions.” *Glia*, vol. 66, no. 11, 22 May 2018, pp. 2340–2352., doi:10.1002/glia.23471.

Figueroa, Maria E., et al. “Leukemic IDH1 and IDH2 Mutations Result in a Hypermethylation Phenotype, Disrupt TET2 Function, and Impair Hematopoietic Differentiation.” *Cancer Cell*, vol. 18, no. 6, 9 Dec. 2010, pp. 553–567., doi:10.1016/j.ccr.2010.11.015.

Gaietta, G., et al. “Multicolor and Electron Microscopic Imaging of Connexin Trafficking.” *Science*, vol. 296, no. 5567, 19 Apr. 2002, pp. 503–507., doi:10.1126/science.1068793.

Gemel, Joanna, et al. “Connecting Exosomes and Connexins.” *Cancers*, vol. 11, no. 4, 4 Apr. 2019, pp. 476–486., doi:10.3390/cancers11040476.

Giepmans, Ben N.G. “Gap Junctions and Connexin-Interacting Proteins.” *Cardiovascular Research*, vol. 62, no. 2, 10 Dec. 2003, pp. 233–245., doi:10.1016/j.cardiores.2003.12.009.

Giepmans, Ben N.G., and Wouter H. Moolenaar. “The Gap Junction Protein connexin43 Interacts with the Second PDZ Domain of the Zona Occludens-1 Protein.” *Current Biology*, vol. 8, no. 16, 27 July 1998, pp. 931–934., doi:10.1016/s0960-9822(07)00375-2.

“Glioblastoma Multiforme.” *Neurosurgical Conditions and Treatments*, American Association of Neurological Surgeons, 2019.

Hammond, Scott M. “Dicing and slicing: The core machinery of the RNA interference pathway.” *FEBS Letters*, vol. 579, no. 26, 31 Oct. 2005, pp. 5822–5829., doi:10.1016/j.febslet.2005.08.079.

Huang, Tingting, et al. “The Physiological Role of Motin Family and Its Dysregulation in Tumorigenesis.” *Journal of Translational Medicine*, vol. 16, no. 1, 12 Apr. 2018, pp. 1–13., doi:10.1186/s12967-018-1466-y.

Izdebska, Magdalena, et al. “The Role of Actin Dynamics and Actin-Binding Proteins Expression in Epithelial-to-Mesenchymal Transition and Its Association with Cancer Progression and Evaluation of Possible Therapeutic Targets.” *BioMed Research International*, vol. 2018, 2018, pp. 1–13., doi:10.1155/2018/4578373.

Kang, Chunsheng, et al. “Silencing Epidermal Growth Factor Receptor by RNA Interference in Glioma.” *Gene Therapy of Cancer Methods in Molecular*

Biology™, vol. 542, 24 Feb. 2009, pp. 335–349., doi:10.1007/978-1-59745-561-9_18.

Kaur, Balveen, et al. "Hypoxia and the Hypoxia-Inducible-Factor Pathway in Glioma Growth Andangiogenesis." *Neuro-Oncology*, vol. 7, no. 2, 1 Apr. 2005, pp. 134–153., doi:10.1215/s1152851704001115.

Kickingereder, Philipp, et al. "IDH Mutation Status Is Associated with a Distinct Hypoxia/Angiogenesis Transcriptome Signature Which Is Non-Invasively Predictable with RCBV Imaging in Human Glioma." *Scientific Reports*, vol. 5, no. 1, 5 Nov. 2015, pp. 1–9., doi:10.1038/srep16238.

Kim, Daniel H., and John J. Rossi. "RNAi Mechanisms and Applications." *BioTechniques*, vol. 44, no. 5, Apr. 2008, pp. 613–616., doi:10.2144/000112792.

Komiya, Yuko, and Raymond Habas. "Wnt Signal Transduction Pathways." *Organogenesis*, vol. 4, no. 2, Apr. 2008, pp. 68–75., doi:10.4161/org.4.2.5851.

Kotini, Maria, and Roberto Mayor. "Connexins in Migration during Development and Cancer." *Developmental Biology*, vol. 401, no. 1, 18 Dec. 2014, pp. 143–151., doi:10.1016/j.ydbio.2014.12.023.

Laing, James G., and Eric C. Beyer. "The Gap Junction Protein Connexin43 Is Degraded via the Ubiquitin Proteasome Pathway." *Journal of Biological Chemistry*, vol. 270, no. 44, 3 Nov. 1995, pp. 26399–26403., doi:10.1074/jbc.270.44.26399.

Laing, James G., et al. "Degradation of Connexin43 Gap Junctions Involves Both the Proteasome and the Lysosome." *Experimental Cell Research*, vol. 236, no. 2, 1 Nov. 1997, pp. 482–492., doi:10.1006/excr.1997.3747.

Laing, James G., et al. “ZO-1 Alters the Plasma Membrane Localization and Function of Cx43 in Osteoblastic Cells.” *Journal of Cell Science*, vol. 118, no. 10, 15 Feb. 2005, pp. 2167–2176., doi:10.1242/jcs.02329.

Laird, Dale W. “Life Cycle of Connexins in Health and Disease.” *Biochemical Journal*, vol. 394, no. 3, 10 Jan. 2006, pp. 527–543., doi:10.1042/bj20051922.

Lamiche, Coralie, et al. “The Gap Junction Protein Cx43 Is Involved in the Bone-Targeted Metastatic Behaviour of Human Prostate Cancer Cells.” *Clinical & Experimental Metastasis*, vol. 29, no. 2, 12 Nov. 2011, pp. 111–122., doi:10.1007/s10585-011-9434-4.

Leithe, E. “Epidermal Growth Factor Regulates Ubiquitination, Internalization and Proteasome-Dependent Degradation of connexin43.” *Journal of Cell Science*, vol. 117, no. 7, 1 Mar. 2004, pp. 1211–1220., doi:10.1242/jcs.00951.

Llaguno, Sheila R Alcantara, and Luis F Parada. “Cell of Origin of Glioma: Biological and Clinical Implications.” *British Journal of Cancer*, vol. 115, no. 12, 10 Nov. 2016, pp. 1445–1450., doi:10.1038/bjc.2016.354.

Macdonald, Bryan T., et al. “Wnt/β-Catenin Signaling: Components, Mechanisms, and Diseases.” *Developmental Cell*, vol. 17, no. 1, July 2009, pp. 9–26., doi:10.1016/j.devcel.2009.06.016.

Maekawa, M. “Signaling from Rho to the Actin Cytoskeleton Through Protein Kinases ROCK and LIM-Kinase.” *Science*, vol. 285, no. 5429, 6 Aug. 1999, pp. 895–898., doi:10.1126/science.285.5429.895.

Molenaar, Remco J., et al. “Correction: Wild-Type and Mutated IDH1/2 Enzymes and Therapy Responses.” *Oncogene*, vol. 37, no. 43, 23 Aug. 2018, pp. 5810–5810., doi:10.1038/s41388-018-0455-1.

Nuriya, Mutsuo, et al. “Norepinephrine Induces Rapid and Long-Lasting Phosphorylation and Redistribution of Connexin 43 in Cortical Astrocytes.” *Biochemical and Biophysical Research Communications*, vol. 504, no. 4, 11 Sept. 2018, pp. 690–697., doi:10.1016/j.bbrc.2018.09.021.

Ohtake, Fumiaki, et al. “K63 Ubiquitylation Triggers Proteasomal Degradation by Seeding Branched Ubiquitin Chains.” *Proceedings of the National Academy of Sciences*, vol. 115, no. 7, 29 Jan. 2018, pp. 1401–1408., doi:10.1073/pnas.1716673115.

Oliveira, Roxane, et al. “Contribution of Gap Junctional Communication between Tumor Cells and Astroglia to the Invasion of the Brain Parenchyma by Human Glioblastomas.” *BMC Cell Biology*, vol. 6, no. 7, 16 Feb. 2005, pp. 1–17., doi:10.1186/1471-2121-6-7.

Oyamada, Masahito, et al. “Regulation of Connexin Expression by Transcription Factors and Epigenetic Mechanisms.” *Biochimica Et Biophysica Acta (BBA) - Biomembranes*, vol. 1828, no. 1, 4 Jan. 2012, pp. 118–133., doi:10.1016/j.bbamem.2011.12.031.

Padrick, S. B., et al. “Arp2/3 Complex Is Bound and Activated by Two WASP Proteins.” *Proceedings of the National Academy of Sciences*, vol. 108, no. 33, 16 Aug. 2011, pp. 472–479., doi:10.1073/pnas.1100236108.

Polakis, Paul. “Wnt Signaling in Cancer.” *Cold Spring Harbor Perspectives in Biology*, vol. 4, no. 5, 20 May 2012, pp. 1–13., doi:10.1101/cshperspect.a008052.

Schadzek, Patrik, et al. “Concatenation of Human Connexin26 (hCx26) and Human Connexin46 (hCx46) for the Analysis of Heteromeric Gap Junction Hemichannels and Heterotypic Gap Junction Channels.” *International Journal of Molecular Sciences*, vol. 19, no. 9, 13 Sept. 2018, p. 2742., doi:10.3390/ijms19092742.

Shao, Qing, et al. “Down-Regulation of Cx43 by Retroviral Delivery of Small Interfering RNA Promotes an Aggressive Breast Cancer Cell Phenotype.” *Cancer Research*, vol. 65, no. 7, 1 Apr. 2005, pp. 2705–2711., doi:10.1158/0008-5472.can-04-2367.

Sin, Wun-Chey, et al. “Opposing Roles of connexin43 in Glioma Progression.” *Biochimica Et Biophysica Acta (BBA) - Biomembranes*, vol. 1818, no. 8, 2012, pp. 2058–2067., doi:10.1016/j.bbamem.2011.10.022.

Sirnes, Solveig, et al. “Connexin43 Acts as a Colorectal Cancer Tumor Suppressor and Predicts Disease Outcome.” *International Journal of Cancer*, vol. 131, no. 3, 12 July 2011, pp. 570–581., doi:10.1002/ijc.26392.

Smyth, James W., et al. “Actin Cytoskeleton Rest Stops Regulate Anterograde Traffic of Connexin 43 Vesicles to the Plasma Membrane.” *Circulation Research*, vol. 110, no. 7, 30 Mar. 2012, pp. 978–989., doi:10.1161/circresaha.111.257964.

Sorgen, P.L, et al. “Structural changes in the carboxyl terminus of gap junction protein connexin43 indicates signaling between binding domains for c-Src and zonula occludes-1.” *Journal of Biological Chemistry*, vol. 41, pp. 544695-54701., doi:10.1074/jbc.M409552200

Spagnol, Gaelle, et al. “Connexin43 Carboxyl-Terminal Domain Directly Interacts with β-Catenin.” *International Journal of Molecular Sciences*, vol. 19, no. 6, 24 May 2018, pp. 1562–1574., doi:10.3390/ijms19061562.

Sulkowski, Parker L., et al. “2-Hydroxyglutarate Produced by Neomorphic IDH Mutations Suppresses Homologous Recombination and Induces PARP Inhibitor Sensitivity.” *Science Translational Medicine*, vol. 9, no. 375, 1 Feb. 2017, pp. 1–32., doi:10.1126/scitranslmed.aal2463.

Tapon, N. “Rho, Rac and Cdc42 GTPases Regulate the Organization of the Actin Cytoskeleton.” *Current Opinion in Cell Biology*, vol. 9, no. 1, 1997, pp. 86–92., doi:10.1016/s0955-0674(97)80156-1.

Tojkander, Sari, et al. “Actin Stress Fibers - Assembly, Dynamics and Biological Roles.” *Journal of Cell Science*, vol. 125, no. 8, 2012, pp. 1855–1864., doi:10.1242/jcs.098087.

Truebestein, Linda, et al. “A Molecular Ruler Regulates Cytoskeletal Remodelling by the Rho Kinases.” *Nature Communications*, vol. 6, no. 1, 1 Dec. 2015, pp. 1–13., doi:10.1038/ncomms10029.

Tsai, Cheng-Fang, et al. “Inhibition of Estrogen Receptor Reduces Connexin 43 Expression in Breast Cancers.” *Toxicology and Applied Pharmacology*, vol. 338, 23 Nov. 2017, pp. 182–190., doi:10.1016/j.taap.2017.11.020.

Uzu, Miaki, et al. “Conflicting Roles of Connexin43 in Tumor Invasion and Growth in the Central Nervous System.” *International Journal of Molecular Sciences*, vol. 19, no. 4, 11 Apr. 2018, pp. 1159–1174., doi:10.3390/ijms19041159.

Wahl, S.M., et al. “Role of Growth Factors in Inflammation and Repair.” *Journal of Cellular Biochemistry*, vol. 40, no. 2, June 1989, pp. 193-199., doi:10.1002/jcb.240400208.

Walgren, Richard A, and Howard L Mcleod. “Small Inhibitory RNA – a Tool for Credentialing Candidate Genes.” *Pharmacogenomics*, vol. 6, no. 3, 24 Nov. 2005, pp. 281–292., doi:10.1517/14622416.6.3.281.

Wang, Chenji, et al. “The Nedd4-like Ubiquitin E3 Ligases Target Angiomotin/p130 to Ubiquitin-Dependent Degradation.” *Biochemical Journal*, vol. 444, no. 2, 2012, pp. 279–289., doi:10.1042/bj20111983.

Wang, Hong-Rui, et al. “Degradation of RhoA by Smurf1 Ubiquitin Ligase.” *Methods in Enzymology Regulators and Effectors of Small GTPases: Rho Family*, vol. 406, 2006, pp. 437–447., doi:10.1016/s0076-6879(06)06032-0.

Wang, Wenqi, et al. “Angiomotin-like Proteins Associate with and Negatively Regulate YAP1.” *Journal of Biological Chemistry*, vol. 286, no. 6, 27 Dec. 2010, pp. 4364–4370., doi:10.1074/jbc.c110.205401.

Watson, Joanna R., et al. “Cdc42 In Actin Dynamics: An Ordered Pathway Governed by Complex Equilibria and Directional Effector Handover.” *Small GTPases*, vol. 8, no. 4, 11 Aug. 2016, pp. 237–244., doi:10.1080/21541248.2016.1215657.

Wei, Jianxin, et al. “A New Mechanism of RhoA Ubiquitination and Degradation: Roles of SCF FBXL19 E3 Ligase and Erk2.” *Biochimica Et Biophysica Acta (BBA) - Molecular Cell Research*, vol. 1833, no. 12, 18 July 2013, pp. 2757–2764., doi:10.1016/j.bbamcr.2013.07.005.

Wu, Jun-I, and Lu-Hai Wang. “Emerging Roles of Gap Junction Proteins Connexins in Cancer Metastasis, Chemoresistance and Clinical Application.” *Journal of Biomedical Science*, vol. 26, no. 1, 14 Jan. 2019, pp. 1–14., doi:10.1186/s12929-019-0497-x.

Xu, Hong-Tao, et al. “Connexin 43 Recruits E-Cadherin Expression and Inhibits the Malignant Behaviour of Lung Cancer Cells.” *Folia Histochemica Et Cytobiologica*, vol. 46, no. 3, 6 Dec. 2008, pp. 315–321., doi:10.2478/v10042-008-0057-9.

Yin, Xiang, et al. “Roles of Astrocytic Connexin-43, Hemichannels, and Gap Junctions in Oxygen-Glucose Deprivation/Reperfusion Injury Induced Neuroinflammation and the Possible Regulatory Mechanisms of Salvianolic Acid B and Carbenoxolone.” *Journal of Neuroinflammation*, vol. 15, no. 97, 27 Mar. 2018, doi:10.1186/s12974-018-1127-3.

Zanconato, Francesca, et al. “YAP/TAZ at the Roots of Cancer.” *Cancer Cell*, vol. 29, no. 6, 13 June 2016, pp. 783–803., doi:10.1016/j.ccell.2016.05.005.

Zhang, Ao, et al. “Connexin 43 Expression Is Associated with Increased Malignancy in Prostate Cancer Cell Lines and Functions to Promote Migration.” *Oncotarget*, vol. 6, no. 13, 23 Mar. 2015, pp. 1–12., doi:10.18632/oncotarget.3449.

Zhou, Jade Z., and Jean X. Jiang. “Gap Junction and Hemichannel-Independent Actions of Connexins on Cell and Tissue Functions - An Update.” *FEBS Letters*, vol. 588, no. 8, 14 Jan. 2014, pp. 1186–1192., doi:10.1016/j.febslet.2014.01.001.

Zhu, Guoqing, et al. “12-O-Tetradecanoylphorbol-13-Acetate (TPA) Is Anti-Tumorigenic in Liver Cancer Cells via Inhibiting YAP through AMOT.” *Scientific Reports*, vol. 7, no. 1, 21 Mar. 2017, pp. 44940–44951., doi:10.1038/srep44940.

Curriculum Vitae

NICHOLAS FREDERICK DOWNING

EDUCATION

Indiana University Indianapolis, IN

Master of Science, Biochemistry and Molecular Biology **October 2019**

DePauw University Greencastle, IN

Bachelor of Arts, Cellular and Molecular Biology **May 2018**

Magna Cum Laude, Minors in Biochemistry and Spanish

PUBLICATIONS

Under Review: "Failure of care acquisition: influential risk factors in American health care inequality"

ACADEMIC EXPERIENCES

12th International Conference on Health Policy Statistics **January 11, 2018**

Poster Presentation Participant: "Failure of care acquisition: influential risk factors in American health disparities."

Midstates Conference for Undergraduate Research in Computer Science and Mathematics **November 18, 2017**

Poster Presentation Participant: "Assessing the risk factors of an individual's decision not to receive essential health care in the United States."

FELLOWSHIPS AND AWARDS

DePauw University Summer Research Fellowship **May 2017 – August 2017**

DePauw University Faculty Distinguished Student Scholarship **2014 – 2018**